Provided for non-commercial research and education use.
Not for reproduction, distribution or commercial use.

This article appeared in a journal published by Elsevier. The attached copy is furnished to the author for internal non-commercial research and education use, including for instruction at the authors institution and sharing with colleagues.

Other uses, including reproduction and distribution, or selling or licensing copies, or posting to personal, institutional or third party websites are prohibited.

In most cases authors are permitted to post their version of the article (e.g. in Word or Tex form) to their personal website or institutional repository. Authors requiring further information regarding Elsevier's archiving and manuscript policies are encouraged to visit:

http://www.elsevier.com/copyright

Author's personal copy

Journal of Asian Earth Sciences 44 (2012) 149–168

Contents lists available at ScienceDirect

Journal of Asian Earth Sciences

journal homepage: www.elsevier.com/locate/jseaes

Late Palaeozoic and Meso-Cenozoic tectonic evolution of the southern Kyrgyz Tien Shan: Constraints from multi-method thermochronology in the Trans-Alai, Turkestan-Alai segment and the southeastern Ferghana Basin

J. De Grave [a,*], S. Glorie [a], A. Ryabinin [b,1], F. Zhimulev [b], M.M. Buslov [b], A. Izmer [c], M. Elburg [a], F. Vanhaecke [c], P. Van den haute [a]

[a] Department of Mineralogy and Petrology, Ghent University, Ghent, Belgium
[b] Institute of Geology and Mineralogy, Siberian Branch, Russian Academy of Sciences, Novosibirsk, Russian Federation
[c] Department of Analytical Chemistry, Ghent University, Ghent, Belgium

ARTICLE INFO

Article history:
Available online 28 April 2011

Keywords:
Zircon U/Pb dating
LA-ICP-MS
Apatite
Thermochronology
Alai
Tien Shan
Pamir

ABSTRACT

In this paper we present new geochronological and thermochronological data from the Turkestan-Alai segment of the southern Kyrgyz Tien Shan, the Ferghana Basin transition and the Trans-Alai Pamir foreland. In the southern and central parts of the Alai Range, towards the Alai Valley, mainly post-collisional granitoids were targeted for zircon U/Pb dating by Laser Ablation-Inductively Coupled Plasma-Mass Spectrometry (LA-ICP-MS), apatite fission-track (AFT) and apatite (U–Th–Sm)/He (AHe) thermochronology. These granitoids, and their thermally metamorphosed contact aureole, yielded Middle Permian zircon crystallization ages of 284 ± 4 to 264 ± 5 Ma. AFT ages (both using the traditional external detector approach as well as using LA-ICP-MS) for these samples are constrained to the Miocene and range between 22.3 ± 1.1 and 8.4 ± 0.3 Ma, while the AHe ages are somewhat younger, between 12.5 ± 0.8 and 5.0 ± 0.3 Ma. This low-temperature thermochronological data suggests an Early Miocene onset of denudation in this area in the Tien Shan orogen, continuing through the Miocene and Pliocene. This denudation is interpreted as a response to reactivation of the mountain belt in the framework of India–Eurasia convergence, and specific to this region, of the Pamir–Tien Shan interaction. On the northern slopes of the Alai Range, at the edge of the Ferghana Basin, a Late Palaeozoic conglomerate yielded a reset Early Cretaceous AFT age of 118 ± 7 Ma, pointing to an older denudation event with respect to those identified in the southern and central parts of the Alai Range. A Mesozoic sediment sample from the same region only contains a Late Triassic age component of ~223 Ma. Mesozoic and Cenozoic age components on the other hand are all detected in the Cenozoic sediments of the Trans-Alai Range, at the transition between the southern Alai Valley and the Pamirs, revealing several Meso-Cenozoic denudation events in the adjoining basement source rocks. The age components in these detrital apatites are ~207 Ma, ~75 Ma, ~18 Ma and ~3 Ma.

© 2011 Elsevier Ltd. All rights reserved.

1. Introduction and Geological Setting

The Tien Shan are the southernmost unit of the Central Asian Orogenic Belt (CAOB). The eastern segment of the Tien Shan is located in China, and the western segment for the most part in the Republic of Kyrgyzstan (Fig. 1). Other parts still are in Uzbekistan, Tajikistan and Kazakhstan. The CAOB is a Palaeozoic accretionary orogen, composed of a multitude of different Precambrian and Palaeozoic units. These amalgamated between Siberia, Baltica and Tarim due to progressive closure of several oceanic basins, in the same fashion as its modern analogue of the circum-Pacific (Windley et al., 2007). By the Permian, the accretionary tectonics in the CAOB culminated as all major composing units were joined. Late- and post-orogenic deformation and magmatism further shaped the CAOB basement architecture and the ancestral Tien Shan in particular (e.g. Allen et al., 1992; Carroll et al., 1995; Gao et al., 1998; Heubeck, 2001; Windley et al., 2007; Xiao et al., 2010). Evidence for widespread Late Carboniferous to Permian strike-slip deformation and shearing and rotation (Allen et al., 1995; Laurent-Charvet et al., 2002; Buslov et al., 2003b), and thus oroclinical bending (Van der Voo et al., 2006) are prevalent throughout the region, as is the presence of contemporaneous post-collisional granitoids (e.g. Konopelko et al., 2007, 2008; Solomovich, 2007). After final construction, the CAOB was subjected to several phases of Mesozoic deformation and was again reactivated in the Late Cenozoic as a distant effect of the

* Corresponding author.
E-mail address: Johan.DeGrave@UGent.be (J. De Grave).
[1] In loving memory of Alexander "Sasha" Ryabinin, 4 January 1984–7 January 2010.

1367-9120/$ - see front matter © 2011 Elsevier Ltd. All rights reserved.
doi:10.1016/j.jseaes.2011.04.019

Author's personal copy

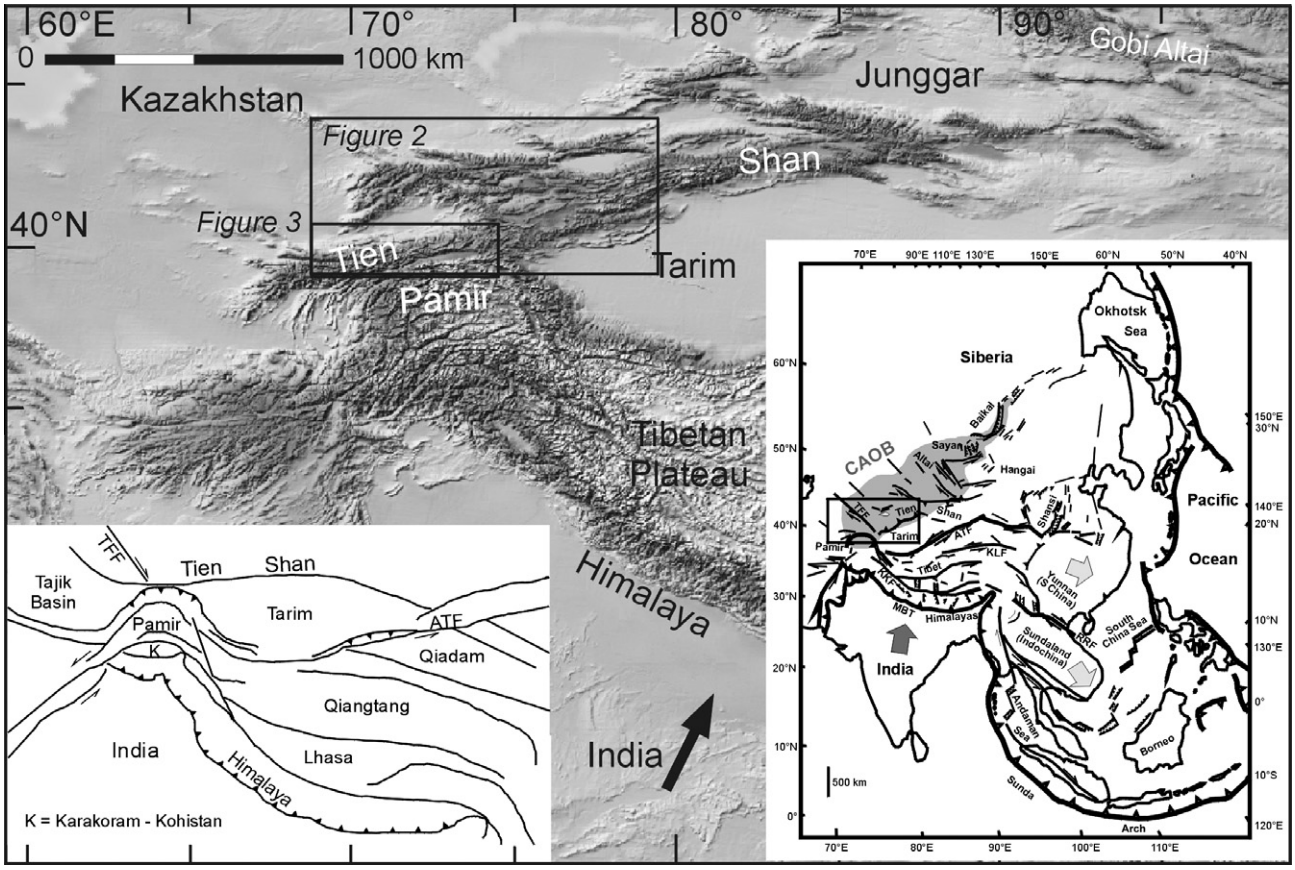

Fig. 1. General location of the Tien Shan in the Central Asian Orogenic Belt (CAOB – inset). The box indicates the location of the study area and corresponds to the geological map area depicted in Fig. 3. A structural scheme of the Tien Shan–Pamir–Tibet area is also shown. TFF = Talas-Ferghana fault, ATF = Altyn Tagh fault.

India–Eurasia collision (e.g. Molnar and Tapponnier, 1975; Otto, 1997; De Grave et al., 2007). Both the Mesozoic and Cenozoic reactivation episodes occurred in an intracontinental setting, as far-field effects of deformation at the (Eur)Asian margins. Tectonic inheritance and basement structure play a prominent role in the partitioning of strain to the interior parts of the CAOB and the Tien Shan in particular (Allen and Vincent, 1997). In this way the CAOB represents the world's largest and most active intracontinental orogenic system with the Tien Shan as an active mountain belt within that context.

The current topography and active structures and mountain ranges of the Kyrgyz Tien Shan mimic its basement architecture. Both the mountain ranges and basement units mostly trend in east–west direction. Based on this structure, the Kyrgyz Tien Shan can be divided in three sections: the Northern (NTS), Central or Middle (MTS) and Southern Tien Shan (STS) (Fig. 2). In literature these sections often carry several different names. Especially when correlating Kyrgyz Tien Shan with Chinese Tien Shan units this can become confusing. We try to follow the terminology used by Windley et al. (2007) and Biske and Seltmann (2010) as much as possible. The NTS in Kyrgyzstan is characterized by the presence of a presumed Precambrian micro-continental basement on which Palaeozoic continental magmatic arcs and Meso-Cenozoic basins developed. The NTS is vastly intruded by Early Palaeozoic ("Caledonian") granitoids as well as by smaller, more isolated Late Palaeozoic ("Hercynian" or "Variscan") post-collisional plutons (Konopelko et al., 2008; Glorie et al., 2010a). The NTS is separated from the MTS by the Nikolaev Line (Fig. 2), which is sometimes considered to be an Early to Middle Palaeozoic suture, as small ophiolite remnants seem to be associated with it (e.g. Simonov et al., 2008). South of the Nikolaev Line the basement of the MTS is composed of Precambrian crust as well, often linked to peri-Gondwanan micro-continents (Biske and Seltmann, 2010). This basement is covered by Middle-Palaeozoic passive margin sequences. While the characteristic large-scale Early Palaeozoic granitoids of the NTS are far less frequent, Late Palaeozoic post-collisional plutons occur within the MTS (Mao et al., 2004; Chiaradia et al., 2006; Morelli et al., 2007). A second Palaeozoic suture, the ophiolite-bearing Atbashi-Inylchek or South Tien Shan suture separates the MTS from the STS (Fig. 2). The STS represents a Late Palaeozoic collision–accretion system characterized by a complex fold-and-thrust structure (Alekseev et al., 2007; Windley et al., 2007; Biske and Seltmann, 2010). Late Palaeozoic post-collisional plutons occur in this section as well (Solomovich and Trifonov, 2002; Chiaradia et al., 2006; Konopelko et al., 2007, 2009; Solomovich, 2007; Seltmann et al., 2011). The NTS and MTS were added to the palaeo-Kazakhstan microplate during Early and Middle Palaeozoic accretion, while the STS developed in the Late Palaeozoic, as an accretionary belt between palaeo-Kazakhstan and Tarim. This latter, larger accretion event generated the post-collisional, mainly Permian intrusions as outlined above.

These main composing sections of the Tien Shan are cut by the northwest-southeast striking Talas-Ferghana fault zone (TFF), effectively creating an eastern and western zone (Fig. 2). The TFF is a Late Palaeozoic structure that played an important role in the post-orogenic deformation of the ancestral Tien Shan. It was clearly reactivated in the Meso-Cenozoic as demonstrated by the right-lateral offset of about 200 km of the Palaeozoic units. Current GPS observations confirm that the fault is still active with dextral slip-rates of about 10–20 mm/a (Burtman et al., 1996). The

Author's personal copy

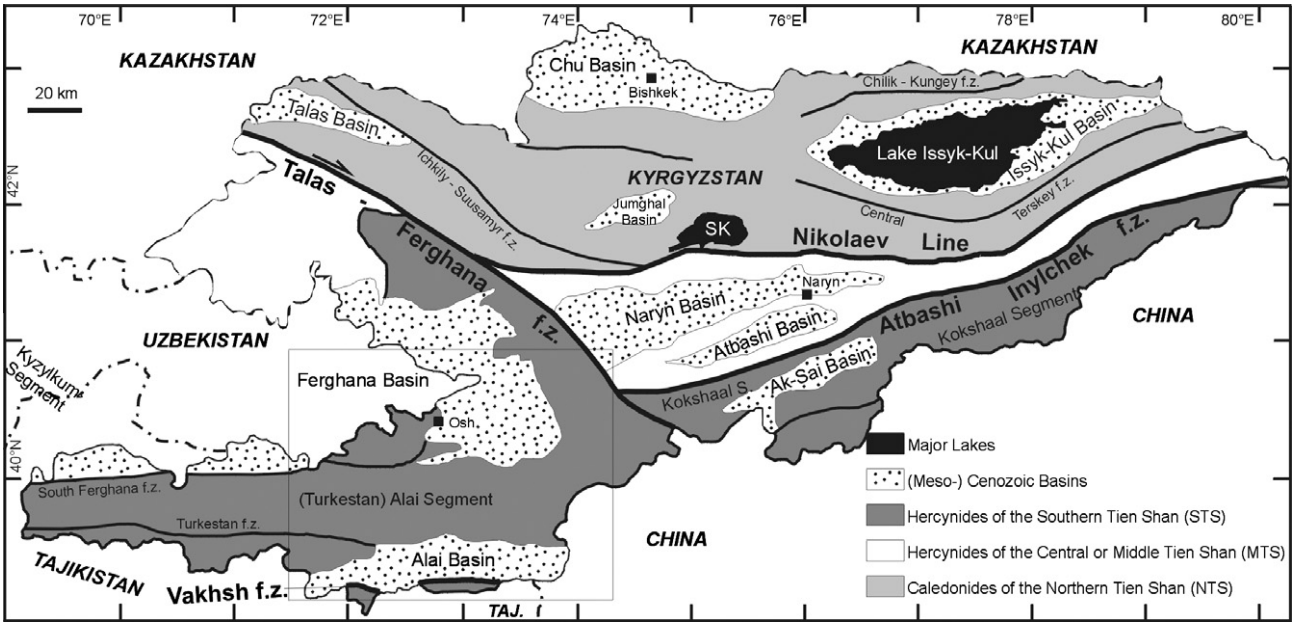

Fig. 2. The Northern (NTS), Central or Middle (MTS), and Southern Tien Shan (STS) units of the Kyrgyz Tien Shan, cut by the Talas-Ferghana fault zone (after Jenchuraeva et al., 2001). The STS study area is shown by the box. The STS unit on former Soviet territory is traditionally subdivided in three segments from east to west. In Kyrgyzstan the Kokshaal segment (east) is separated from the (Turkestan) Alai Segment (west) by the Talas-Ferghana fault zone. The Kyzylkum Segment of STS is the part of this unit located in Uzbekistan. SK = Song-Kul Lake; it occupies a basin on top of Song-Kul plateau.

Palaeozoic units west of the TFF are hence displaced relative to the north with respect to their counterparts east of the fault. In this paper we present new geochronologic and thermochronologic data that constrains the Late Palaeozoic to Recent evolution of the STS block, west of TFF. This part of the Kyrgyz Tien Shan is also known as the Turkestan-Alai section or Alai segment and supports the present-day Turkestan, Alai, and Kichi-Alai mountain ranges with peaks up to 5500 m a.s.l (Fig. 3). To the south of these ranges the Alai Valley or Alai Basin is situated. This is an intramontane sedimentary basin of an average elevation of 2700 m (3200–3500 m from north to south in our study area, Fig. 3), capturing the Meso-Cenozoic sediments shed from the STS (to the north) and the advancing Pamir thrust nappes (to the south). The now intramontane Alai Basin once formed a corridor linking the Tarim Basin (east) with the Tajik Basin (west) in the pre-Late Cenozoic (Strecker et al., 2003). The STS and Alai Basin are separated from the leading edge of the Pamirs, the Trans-Alai Range, by the Vakhsh fault zone (Fig. 2), presently a reactivated thrust fault system (Main Pamir Thrust, MPT). The Trans-Alai Range hosts some of the major Pamir peaks such as Ibn Sina peak (peak Lenin, 7134 m) and Ismoil Somoni peak (peak Stalin or Communism peak, 7495 m) for example.

The (Turkestan)-Alai section from which our samples originate, is one of three subdivisions of the STS. Indeed, the STS can be further divided in three segments, an eastern section, the Kokshaal section, is the STS unit in southern Kyrgyzstan, east of the TFF. The western section is the Kyzylkum section and is a part of the STS, located in Uzbekstan. The (Turkestan)-Alai section is the central section in between Kokshaal and Kyzylkum (Biske and Seltmann, 2010; Seltmann et al., 2011; Fig. 2).

During the Mesozoic, the entire orogen of the ancestral Tien Shan was subjected to protracted reactivation, building an effective physiographic barrier between the Junggar and Kazakhstan Basins to the north and the Tarim Basin to the south (Graham et al., 1993; Hendrix, 2000). The Junggar and Tarim Basins acted as foreland basins to the evolving orogen. These foreland basins as well as Mesozoic intramontane Tien Shan basins record several coarse, clastic sediment pulses with angular unconformaties at their base. These sediment records point toward successive distinct orogenic phases in the Late Triassic (–Early Jurassic), Late Jurassic–Early Cretaceous, and the Late Cretaceous (Hendrix et al., 1992; Allen et al., 1993; Vincent and Allen, 2001). The driving forces for these successive reactivation events are thought to be contemporaneous with collision–accretion events transpiring at the margins of the growing (Eur)Asian continent. During the Mesozoic several so-called Cimmerian blocks (peri-Gondwanan fragments) docked with (Eur)Asia as several tracts of the (Palaeo-)Tethys Ocean lithosphere were consumed by progressing subduction. Several of these blocks (such as the Tibetan blocks Qiangtang, Lhasa and others) were ultimately pulled in the subduction zone and collided with the southern Eurasian active margin in a punctuated fashion throughout the Mesozoic era (e.g. Otto, 1997; Yin and Harrison, 2000; Schwab et al., 2004; Kapp et al., 2007, and references therein). It is thought that these collisions, which together comprise the Cimmerian orogeny, propagated deformation to the north, and in this way reactivated structures in the Tien Shan belt (e.g. Graham et al., 1993; Allen and Vincent, 1997; Vincent and Allen, 2001; De Grave et al., 2007). In this context, the Pamir indenter played a pivotal role as conduit for deformation directly to the Kyrgyz STS terrane.

As mentioned, the Late Cenozoic in the Tien Shan is characterized by a renewed and intense episode of tectonic reactivation due to ongoing India–Eurasia convergence. This reactivation is responsible for the formation of the modern Tien Shan orogen and its topography as it appears today. Evidence for initial growth of the modern Tien Shan is found in foreland and intramontane basins in the form of increased (coarse clastic) sediment rates, and unconformities. These sediments eroded from the growing mountain ranges and advancing thrust nappes and are deposited in these basins from the Late Oligocene onwards, with thick sequences in the Miocene, Pliocene to Recent (e.g. Allen et al., 1993; Cobbold et al., 1994; Yin et al., 1998). From seismological, geophysical and geodetic investigations it is clear the Tien Shan are a recent and active intracontinental mountain belt (e.g. Abdrakhmatov et al., 1996; Omuralieva et al., 2009). The Late Cenozoic reactivation is translated in fold-and-thrust tectonics (Yin et al., 1998; Hubert-Ferrari et al., 2007; Oskin and Burbank, 2007) in the Tien

Author's personal copy

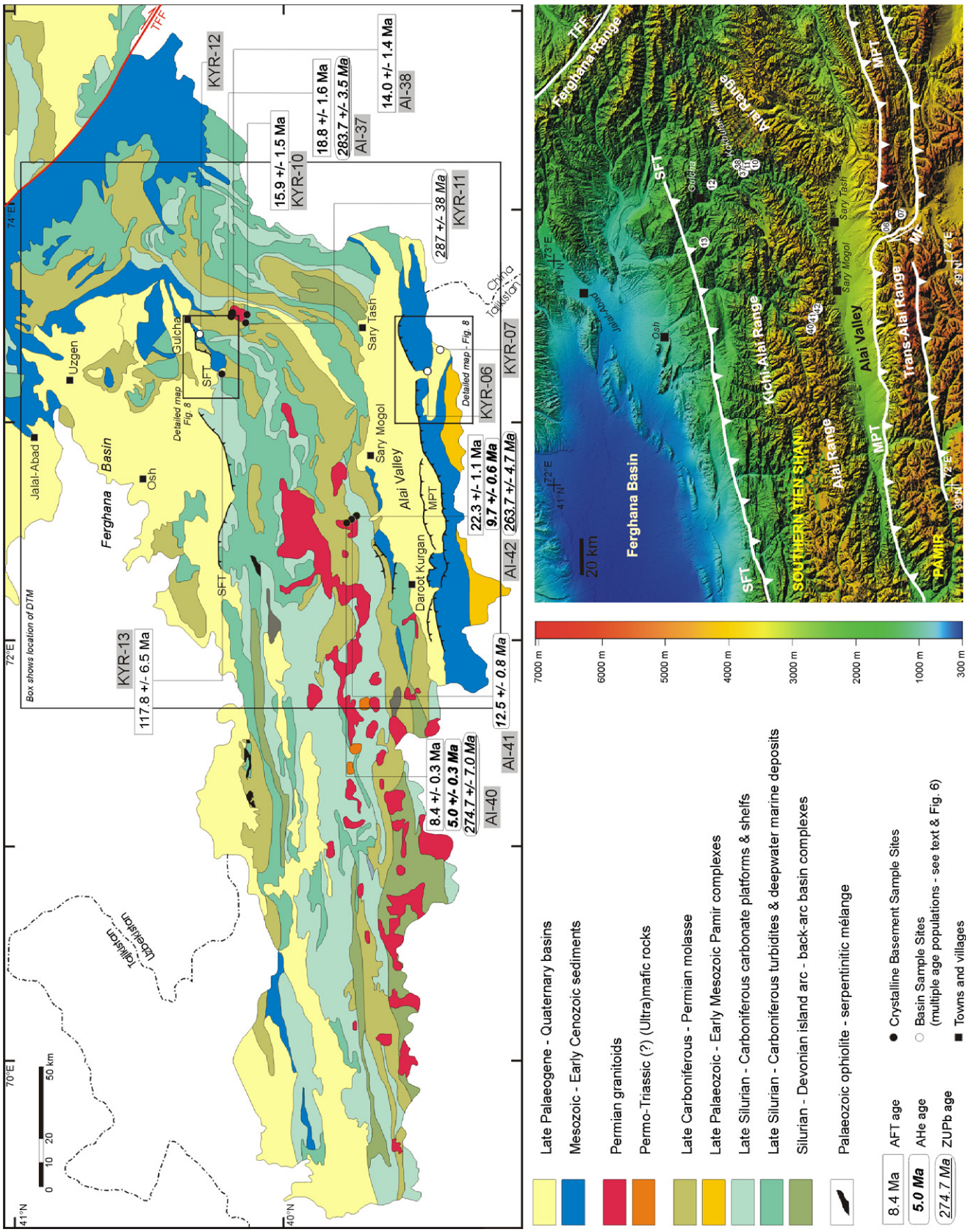

Fig. 3. Simplified geological map of the western section of the Kyrgyz Southern Tien Shan with indication of sample sites and dating results (based on Jenchuraeva et al., 2001 and Tursungaziev and Petrov, 2008). The outlined area is also shown on a digital terrain model (DTM) where basins and ranges are shown (sample sites also indicated). The tectonic structure of the Alai study area is schematically presented on the map and the DTM. MF = Markansu Fault, MPT = Main Pamir Thrust, SFT = South Ferghana Thrust, TFF = Talas-Ferghana fault.

Author's personal copy

Shan ranges, as well as in strike-slip deformation (Burtman et al., 1996; Allen et al., 2001; Buslov et al., 2003a). The continued crustal shortening induced by the indentation of the Indian plate invokes the convergence of the STS with the Tarim microplate (east of TFF) and the Pamirs (west of TFF) (Fig. 2.). The STS are thrust on top of Tarim (Allen et al., 1999; Yang and Liu, 2002), while in our study area, it is the Pamir terrane which is thrust atop the Alai Valley and the STS (Coutand et al., 2002) along the Main Pamir Thrust (MPT) (Fig. 3). In this area, from terrain and geophysical observations, Coutand et al. (2002) identify two stages of Late Cenozoic deformation, a first in the Late Oligocene–Early Miocene, and a second contraction from the Middle Miocene until the present. This is corroborated by findings in the Eastern Pamir (Robinson et al., 2007) and confirms earlier data by e.g. Pavlis et al. (1997) in the Pamir–Tien Shan convergence zone west of the Alai Valley, towards the Gissar area and the Tajik Basin.

2. Samples and methodology

Sample details including locations and lithology are listed in Table 1. Their positions are plotted on a simplified geological map and digital terrain model (Fig. 3). The samples compose a more or less north–south profile across the central Alai Range from the Trans-Alai/Alai Basin (south) to the southern edges of the Ferghana Basin (north). The samples from the Alai Range mainly consist of Late Palaeozoic post-collisional granites and diorites. This type of intrusions are found throughout the Kyrgyz Tien Shan, in all composing terranes (NTS, MTS, and STS), as outlined in the previous section. In the Alai (and Kichi-Alai) Range, they are intruded in a basement of mainly Middle to Late Palaeozoic marine deposits (Pickering et al., 2008. Biske and Seltmann, 2010). Two intrusions of this type were sampled (Table 1, Fig. 3). In the Kokbulak Mountains of the northern-central part of the Alai Range, an intrusive stock close to Murdash was sampled. In fact this intrusion seems to consist of a main northern body and a smaller cupola just south of the main body. Tursungaziev and Petrov (2008) named these intrusions according to local place names as Belauli (Belaulinski) and Askaly (Askalinski) respectively. Samples AI-37 and AI-38 represent a vertical section in the northern part of this pluton, sample KYR-10 is a sample from the southern part. Sample KYR-11 is a quartz-biotite schist from the amphibolite contact aureole of the Belauli and Askaly plutons. It is located in between the KYR-10 and AI-37/AI-38 sample sites. The Middle–Late Palaeozoic sedimentary protolith was subjected to thermal metamorphism during intrusion and post-magmatic cooling of the granitoids. The second intrusion that was sampled for this study, is located in the southern part of the Alai Range, close to the Alai Valley transition. Sample AI-40 comes from this body in the Kashka-Suu valley towards Kindyk Pass and Skobieleva peak. Tursungaziev and Petrov (2008) named the main intrusion here as Dzhaman-Dzhailiuski. Samples AI-41 and AI-42 are from smaller granitic outcrops up the Kashka-Suu valley in between the main Dzhaman-Dzhailiuski and the Sary-Mogol intrusion (somewhat more westwards, Fig. 3). These outcrops probably correspond to a small intrusion labelled by Tursungaziev and Petrov (2008) as the Balyktinski body. AI-42 in fact comes from a felsic dyke associated with this body. Solomovich (2007) calls this larger area of igneous intrusions in this part of the Alai Range as the Karakazyk pluton. Two other, non-granitic samples from the Alai Range were collected near its northern boundary at the South Ferghana Thrust (SFT). KYR-13 is a conglomerate sample containing granitic and other crystalline clasts. It was taken close to Gulcha Village, near Chigirchik pass towards the Ferghana Basin. According to several consulted maps, the conglomerate is from a unit of Late Carboniferous–Permian molasse (Fig. 3), associated with the Late Palaeozoic Tien Shan orogeny. KYR-12, a sandstone sample, was collected closeby, just southwest of Gulcha village, in a unit of Mesozoic sediments of the Ferghana Basin. These sediments are listed from Triassic to Palaeocene depending on the maps consulted. The most detailed description comes from Tursungaziev and Petrov (2008) who base their findings on older 1: 200,000 scale Soviet maps and assign the sediments to the Early to Late Cretaceous transition. They are capped by Late Cretaceous, Cenomanian–Turonian clays and marls that contrary to the older sediments are at least partly considered to be of marine nature. Burtman et al. (1996) for example describe this area, including the Ferghana Basin, to evolve from continental settings to shallow, epicontinental marine environments at that time. Finally, two Neogene sandstones (KYR-06 and 07) from the Alai Basin and Trans Alai Range were sampled near the Tajik border.

The samples were separated using conventional magnetic and heavy liquid techniques. Apatites and zircons were handpicked under a high-resolution zoom-stereomicroscope, avoiding inclusions and impurities as much as possible. They were analyzed using several geochronological and thermochronological techniques in a multi-method approach in order to elucidate the post-amalgamation history of the Tien Shan and of the Alai region of the Kyrgyz Southern Tien Shan in particular. Zircon U/Pb dating (ZUPb) using LA-ICP-MS (Laser Ablation-Inductively Coupled Plasma-Mass Spectrometry) was performed on zircons from the granitic plutons to constrain their crystallization ages and to obtain a high-temperature benchmark for thermochronology analysis of the basement. These "Hercynian" granitoids also have a significance from the viewpoint of ore geology (e.g. Mao et al., 2004; Morelli et al., 2007) and knowledge of their emplacement ages is important in that context as well. Absolute radiometric age information from this region is still scarce. This study presents new ZUPb ages for the granitic bodies described above.

Low-temperature thermochronology was applied on apatites from both the basement and the basin samples. The basement

Table 1
Sample location and lithology details. P_3 = Late Permian, J?–C = Jurassic(?)–Cretaceous, Ng = Neogene.

Sample	Latitude	Longitude	Altitude (m)	Locality	Lithology	Strat.
Palaeozoic "basement" samples						
KYR-10	40°03′59″N	73°32′28″E	2000	Alai Range, Murdash	Diorite	
KYR-11	40°06′50″N	73°31′56″E	1920	Alai Range, Murdash	Q-biotite schist	
KYR-13	40°15′24″N	73°18′21″E	2340	Alai Range, Chigirchik pass	Conglomerate	P_3
AI-37	40°07′47″N	73°31′25″E	1810	Alai Range, Kokbulak	Granite	
AI-38	40°08′22″N	73°32′07″E	1990	Alai Range, Kokbulak	Granodiorite	
AI-40	39°45′50″N	72°34′53″E	4510	Alai Range, Kashka-Suu	Granite	
AI-41	39°42′49″N	72°39′21″E	3560	Alai Range, Kashka-Suu	Diorite	
AI-42	39°42′51″N	72°39′56″E	3100	Alai Range, Kashka-Suu	Granite/dyke	
Meso-Cenozoic basin samples						
KYR-06	39°26′01″N	73°14′55″E	3710	Trans-Alai Range,Kyzyl-Art	Sandstone	Ng up
KYR-07	39°23′12″N	73°19′30″E	4380	Trans-Alai Range,Kyzyl-Art	Sandstone	Ng low
KYR-12	40°15′12″N	73°23′51″E	1825	Alai Range, Gulcha	Sandstone	J?–C

Author's personal copy

samples on one hand include the same granitoids as dated with ZUPb. Both the apatite fission-track (AFT) and Apatite (U–Th–Sm)/He (AHe) thermochronometers were used to constrain the cooling and hence denudation of the basement during the Meso-Cenozoic reactivation events in an absolute time frame. In tandem, detrital apatites from the Meso-Cenozoic sandstone samples from the southeastern Ferghana Basin and the eastern Alai Basin and Trans-Alai Range were analyzed with the AFT method in order to identify the individual cooling age components from the exhumed basement. Both the traditional external detector as well as the LA-ICP-MS approach to AFT dating were employed in this work. A brief account of analytical procedures is given below.

2.1. Zircon U/Pb dating by LA-ICP-MS

Zircons were carefully handpicked, mounted in epoxy and polished. Direct analysis of the zircon grains was accomplished by using laser ablation (LA) for sample introduction. A New Wave UP193HE excimer-based laser ablation system (Fremont, CA, USA) was equipped with a teardrop-shaped low-volume (<2.5 cm^3) ablation cell (Horstwood et al., 2003; Frei and Gerdes, 2009) and coupled to the mass spectrometer. A helium–argon mixture was used as carrier gas, whereby argon was introduced and mixed with the helium after the ablation cell position. Determination of U, Th, and Pb isotope concentrations was carried out using a Thermo Scientific Element XR Sector Field ICP-MS (Bremen, Germany) and isotope ratios were determined. Measurements were performed at the ICP-MS facilities of the Department of Analytical Chemistry, Ghent University and procedures are nearly identical to those described by Glorie et al. (in press). Instrumental details are listed in Table 2.

Data reduction was performed using the PepiAGE-software (Dunkl et al., 2009). Laser-induced elemental fractionation was corrected for by using the arithmetic mean isotopic ratios for each run. Instrumental mass discrimination was corrected by normalization to the reference zircon GJ-1 (Jackson et al., 2004). The drift-correction was done by applying a linear fit through the measured ratios for the GJ-1 standard. The Concordia ages were calculated with Isoplot (Ludwig, 2003). Plešovice (Sláma et al., 2008) and 91500 (Wiedenbeck et al., 1995) secondary zircon standards were measured multiple times throughout each sequence and served as an accuracy check. For the Plešovice zircon standard, our long-term (47 analyses) mean Concordia age yields 338 ± 2 Ma, which is in excellent agreement with the reported ID-TIMS age of 337.1 ± 0.4 Ma (Izmer et al., 2010). The results for all analyzed zircon grains (excluding the outliers; <10%), are listed in Table 3 and resulting Concordia or intercept ages are shown in Fig. 3. Concordia diagrams are presented in Fig. 4.

Table 2
Analytical details for the LA-ICP-MS as used for zircon U/Pb dating and apatite fission-track dating.

ICP-MS	
Brand and model	ThermoFinnigan Element XR (Sector-field MS)
Forward power	800–1000 W
Gas flows (l/min) U/Pb	
Cool (Ar)	16.0
Carrier (Ar)	1.2–1.3
Gas flows (l/min) AFT	
Cool (Ar)	16.0
Carrier (He)	0.3–0.4
Additional (Ar)	0.8–0.9
Laser	
Type of Laser	ArF - Excimer
Brand and model	New Wave UP 193
Ablation cell	Teardrop-shaped low-volume cell (<2.5 cm^3)
Laser wavelength	193 nm
Spot size	30 μm (U/Pb)–15 μm (AFT)
Repetition rate	10 Hz
Nominal energy output	40% (U/Pb)–100% (AFT)
Laser fluency	2.5–3.0 J cm^{-2} (U/Pb) 8.0–8.5 J cm^{-2} (AFT)
Laser warm up (background collection)	25 s (U/Pb)–10 s (AFT)
Ablation time	40 s (400 pulses) (U/Pb)–16 s (160 pulses) (AFT)
Wash-out	25 s (U/Pb)–15 s (AFT)
Ablation mode	Zigzag raster covering counted zone (raster: 60 × 60 μm) (AFT)
Scan speed	15 μm/s (AFT)
Data acquisition parameters	
Resolution mode	Low
Data Acquisition protocol	Time-resolved analysis
Scan mode	E-scan
Scanned masses U/Pb	202 (Hg), 204 (Hg, Pb), 206 (Pb), 207 (Pb), 208 (Pb), 232 (Th), 235 (U), 238 (U)
Scanned masses AFT	44 (Ca), 232 (Th), 235 (U), 238 (U)
Detector deadtime	18 ns
Background collection	25 s (U/Pb)–10 s (AFT)
Ablation for age calculation	40 s (U/Pb)–16 s (AFT)
Wash-out collection	15 s (U/Pb)–10 s (AFT)
Standardization and data reduction U/Pb	
Reference standard used	GJ-1
Secondary standard used	Plešovice
Data reduction software used	PepiAGE-software (Dunkl et al., 2009) + In house Excel-spreadsheet
Standardization and data reduction AFT	
Reference standard used	NIST 610–NIST 612
Secondary standard used	Durango Apatite
Internal standard	^{44}Ca[a]
Data reduction software used	In house Excel-spreadsheet

[a] NIST, DUR: published values (GEOREM preferred values – Jochum and Stoll, 2008; Seifert et al., 2000). Unknowns: average SEM-EDX measured values, calibrated against DUR reference value.

2.2. Apatite fission-track thermochronology

The apatite fission-track (AFT) method is a low-temperature thermochronological technique based on the spontaneous fission decay of ^{238}U. Depending on the chemical composition of the apatite (especially Cl/F ratio, Green et al., 1986; Carlson et al., 1999) fission tracks in apatite become partially stable when cooled to about 125–100 °C. At these temperatures the tracks are shortened and their original length still decreases (partial annealing). When temperatures reach ~60 °C the tracks in apatite are thought to be stable (Wagner and Van den haute, 1992 and references therein) although some annealing at ambient temperatures might take place. Together with the AFT age, track length distributions form an important tool in AFT thermochronology (Gleadow et al., 1986). The analytical procedures for AFT dating applied in this paper consist of two different techniques. A first technique is the traditional external detector method where apatite mounts are covered with an U-free external muscovite mica detector and then irradiated with thermal neutrons to produce induced ^{235}U fission tracks. Details on the procedures used in our laboratory can be found in De Grave and Van den haute (2002) and De Grave et al. (2009) for example, and are briefly outlined below.

Apatites from samples KYR-10, KYR-13, AI-40, and AI-42 were embedded in epoxy, polished and analyzed with the 'traditional' external detector (ED) method (Table 4). Spontaneous tracks were etched with a 2.5% HNO_3 solution for 70 s at 25 °C, induced tracks in the muscovite ED with 40% HF for 40 min at 20 °C. Irradiation was performed at the Belgian Reactor 1 (BR1) facility of the Belgian Nuclear Research Centre in Mol, where the well-thermalized channel (f-ratio of 98) X26 was used (De Grave et al., 2010) and a thermal neutron fluence of 2.23×10^{15} cm^{-2} was achieved. This was monitored using metal activation monitors (diluted Au–Al and Co–Al alloys; Van den haute et al., 1998). AFT ages obtained for aforementioned samples are conventional ζ-ages (Hurford, 1990)

Table 3
Zircon U/Pb dating results by LA-ICP-MS.

n	^{207}Pb[a] (cps)	U[b] (ppm)	Pb[b] (ppm)	Th[b]/U	$^{206}Pb/^{204}Pb$	$^{206}Pb^{c}/^{238}U$	±2σ (%)	$^{207}Pb^{c}/^{235}U$	±2σ (%)	$^{207}Pb^{c}/^{206}Pb$	±2σ (%)	Rho[d]	$^{206}Pb^{e}/^{238}U$	±2σ (Ma)	$^{207}Pb^{e}/^{235}U$	±2σ (Ma)	Con.[f]
AI-42																	
1	1650	384	16	0.27	6526	0.0413	6.1	0.2931	9.0	0.0515	6.6	0.68	261	15	261	21	100
2	3214	695	29	0.06	6685	0.0427	6.4	0.3211	8.5	0.0546	5.6	0.76	269	17	283	21	105
3	1841	430	18	0.09	1259	0.0427	6.9	0.2986	10.8	0.0507	8.4	0.63	270	18	265	26	98
4	1180	265	11	0.09	1002	0.0418	5.3	0.3151	9.5	0.0547	7.9	0.56	264	14	278	23	105
5	1921	458	18	0.17	3650	0.0397	4.7	0.2912	7.2	0.0532	5.4	0.66	251	12	259	17	103
6	2647	601	25	0.07	1413	0.0429	4.9	0.3116	7.7	0.0527	5.9	0.64	271	13	275	19	102
7	1854	446	19	0.06	989	0.0439	5.5	0.3062	7.1	0.0506	4.5	0.77	277	15	271	17	98
8	3702	817	34	0.11	13,662	0.0420	6.2	0.3174	7.9	0.0548	5.0	0.78	265	16	280	20	106
9	4836	1156	45	0.05	2755	0.0405	6.8	0.3086	8.2	0.0552	4.6	0.83	256	17	273	20	107
10	2471	603	24	0.10	1464	0.0396	7.0	0.2925	8.5	0.0536	4.8	0.83	250	17	260	20	104
11	4675	1128	45	0.06	2598	0.0418	5.7	0.3098	7.7	0.0538	5.1	0.74	264	15	274	19	104
12	3479	795	32	0.15	12,789	0.0419	4.5	0.3145	7.6	0.0545	6.1	0.59	264	12	278	19	105
13	2631	633	26	0.18	2336	0.0424	4.9	0.3034	7.8	0.0519	6.1	0.62	268	13	269	19	101
14	3051	757	33	0.09	875	0.0444	8.5	0.3247	10.7	0.0530	6.5	0.79	280	23	286	27	102
15	4517	1218	48	0.09	1048	0.0398	10.1	0.2954	12.6	0.0539	7.5	0.80	251	25	263	29	105
16	4540	1146	46	0.05	5328	0.0422	6.9	0.3058	9.3	0.0526	6.1	0.75	266	18	271	22	102
17	1607	422	17	0.20	717	0.0406	4.7	0.2836	7.8	0.0506	6.2	0.60	257	12	254	18	99
AI-40																	
1	6584	1594	70	0.13	24,938	0.0438	5.3	0.3203	6.6	0.0530	3.9	0.80	276	14	282	16	102
2	6572	1697	73	0.12	2334	0.0418	5.7	0.2999	7.4	0.0520	4.6	0.78	264	15	266	17	101
3	6023	1560	68	0.08	2465	0.0426	5.0	0.2988	7.0	0.0508	5.0	0.71	269	13	265	17	99
4	4122	971	46	0.09	1631	0.0461	4.2	0.3270	6.1	0.0514	4.4	0.70	291	12	287	15	99
5	7026	1755	79	0.16	2183	0.0442	5.0	0.3157	6.2	0.0518	3.5	0.82	279	14	279	15	100
6	5090	1203	57	0.23	1715	0.0457	4.7	0.3332	6.1	0.0529	4.0	0.76	288	13	292	16	101
7	5715	1428	61	0.13	2994	0.0425	5.2	0.3185	8.2	0.0543	6.3	0.63	268	14	281	20	105
8	6876	1677	75	0.10	1709	0.0430	6.7	0.3342	9.0	0.0563	5.9	0.75	272	18	293	23	108
9	5346	1433	59	0.12	2582	0.0403	6.2	0.3021	7.5	0.0543	4.1	0.83	255	16	268	18	105
10	5785	1601	68	0.13	1764	0.0424	6.4	0.2987	7.3	0.0511	3.5	0.88	268	17	265	17	99
AI-37																	
1	5292	1430	63	0.11	5191	0.0460	3.9	0.3491	6.3	0.0551	4.9	0.63	290	11	304	17	105
2	5095	1527	66	0.10	20,380	0.0446	4.4	0.3149	6.5	0.0512	4.8	0.68	281	12	278	16	99
3	7488	2175	97	0.14	3008	0.0462	4.3	0.3323	5.7	0.0522	3.7	0.75	291	12	291	15	100
4	5524	1572	66	0.11	6872	0.0435	4.3	0.3276	6.4	0.0546	4.7	0.67	275	11	288	16	105
5	4919	1499	64	0.06	2342	0.0443	4.7	0.3116	6.6	0.0511	4.7	0.70	279	13	275	16	99
6	6659	1993	82	0.08	4141	0.0438	4.1	0.3184	6.0	0.0528	4.4	0.68	276	11	281	15	102
7	1975	456	23	0.08	37,569	0.0544	4.1	0.3912	7.5	0.0522	6.3	0.54	341	14	335	22	98
8	6315	1911	81	0.10	5404	0.0442	5.1	0.3187	7.1	0.0523	5.0	0.71	279	14	281	18	101
9	8371	2541	107	0.10	11,928	0.0443	4.4	0.3135	6.2	0.0513	4.4	0.70	279	12	277	15	99
10	9863	2777	123	0.30	11,042	0.0449	3.8	0.3316	6.2	0.0536	4.8	0.62	283	11	291	16	103
11	5958	1672	75	0.28	5735	0.0462	3.8	0.3379	5.9	0.0530	4.5	0.64	291	11	296	15	101
12	9770	2760	122	0.10	11,782	0.0459	3.6	0.3352	5.8	0.0530	4.5	0.62	289	10	294	15	101
Kyr-11																	
1	588	77	4	0.43	123	0.0502	5.2	0.5363	14.7	0.0775	13.7	0.35	316	16	436	53	138
2	1027	155	8	0.71	1442	0.0465	2.8	0.3768	11.6	0.0588	11.2	0.25	293	8	325	33	111
3	3301	421	24	0.29	444	0.0510	5.5	0.5146	8.5	0.0733	6.4	0.65	320	17	422	30	132
4	1445	299	17	0.63	737	0.0492	9.8	0.3390	14.3	0.0500	13.7	0.69	310	30	296	37	96
5	1852	219	12	0.24	351	0.0515	5.3	0.5477	15.1	0.0772	14.2	0.35	324	17	443	56	137
6	660	94	5	0.31	111	0.0529	8.1	0.5251	19.7	0.0720	18.0	0.41	332	26	429	71	129
7	7512	610	93	0.61	1246	0.0511	4.5	0.3950	16.2	0.0561	15.5	0.28	321	14	338	48	105
8	2371	513	26	0.20	1361	0.0521	9.4	0.3778	12.4	0.0526	8.1	0.76	327	30	325	35	99
9	840	200	10	0.28	242	0.0498	4.1	0.3400	13.6	0.0495	13.0	0.30	313	12	297	36	95

(*continued on next page*)

Author's personal copy

Author's personal copy

Table 3 (*continued*)

n	$^{207}Pb^{a}$ (cps)	U^{b} (ppm)	Pb^{b} (ppm)	Th^{b}/U	$^{206}Pb/^{204}Pb$	$^{206}Pb^{c}/^{238}U$	±2σ (%)	$^{207}Pb^{c}/^{235}U$	±2σ (%)	$^{207}Pb^{c}/^{206}Pb$	±2σ (%)	Rho[d]	$^{206}Pb^{e}/^{238}U$	±2σ (Ma)	$^{207}Pb^{e}/^{235}U$	±2σ (Ma)	Con.[f]
10	1415	353	18	0.48	1044	0.0455	9.3	0.3437	14.9	0.0548	11.7	0.62	287	26	300	39	105
11	2101	575	27	0.29	567	0.0459	11.3	0.3119	14.8	0.0492	9.1	0.76	290	32	276	36	95
12	1373	289	15	0.31	530	0.0491	6.0	0.4584	11.6	0.0677	10.0	0.51	309	18	383	38	124
13	1627	441	26	0.76	759	0.0519	4.1	0.3864	7.2	0.0540	5.9	0.57	326	13	332	20	102
14	963	252	13	0.38	922	0.0469	5.4	0.3810	12.9	0.0590	11.7	0.42	295	15	328	37	111
15	819	230	13	0.69	5001	0.0511	5.9	0.3801	10.9	0.0539	9.2	0.54	322	18	327	31	102
AI-42	2930	703	29	0.11	3829	0.0418	6.2	0.3054	8.7	0.0530	6.0	0.71	264	16	271	21	103
AI-40	5914	1492	66	0.13	4432	0.0433	5.4	0.3148	7.1	0.0528	4.5	0.77	273	15	278	17	102
AI-37	6436	1859	81	0.13	10,449	0.0457	4.2	0.3318	6.4	0.0527	4.8	0.66	288	12	291	16	101
Kyr-11	1860	315	21	0.44	992	0.0496	6.4	0.4142	13.2	0.0604	11.4	0.50	312	20	350	40	112

[a] Within-run, background-corrected mean ^{207}Pb signal.
[b] U and Pb content and Th/U ratio were calculated relative to the GJ-1 zircon standard.
[c] Corrected for: background, within-run Pb/U fractionation (in case of $^{206}Pb/^{238}U$) and common Pb (using Stacey and Kramers (1975) model Pb composition) and subsequently normalised to GJ-1 (Instrumental drift corrected using a linear fit calibration line). $^{207}Pb/^{235}U$ calculated using $^{207}Pb/^{206}Pb * ^{206}Pb/^{238}U * 137.88$.
[d] Rho is the error correlation defined as $err^{206}Pb/^{238}U/err^{207}Pb/^{235}U$.
[e] U/Pb ages were calculated with Isoplot (Ludwig, 2003).
[f] Degree of concordance = $age^{206}Pb/^{238}U/age^{207}Pb/^{206}Pb \times 100$.

with an overall weighted mean zeta of 253.1 ± 2.4 a cm^2 (Durango and Fish Canyon Tuff apatite standards). The IRMM-540 dosimeter glass (De Corte et al., 1998) was used. Glass shards were regularly spaced in the sample package to detect and correct for any axial thermal neutron fluence gradient and to allow interpolation of induced glass dosimeter track densities (ρ_d) for individual samples.

Where possible 100 natural confined tracks were measured in order to construct an AFT length-frequency distribution, a target that was not always attained. Especially in the young samples, low spontaneous track densities translate in insufficient numbers of measurable horizontal confined tracks. To enhance this number for a representative "young" sample, a duplicate epoxy mount of sample AI-40 (which had the most and the best-quality apatite grains of the "young" samples) was made and wrapped in Al-foil (Al-degrader). This mount was then irradiated with heavy ions at the linear accelerator of the Gesellschaft für Schwerionenforschung (GSI), Darmstadt, Germany. The sample was irradiated with a Au-ion beam from the UNILAC linear accelerator at GSI. Au-ions were accelerated to ~11.4 MeV/amu, corresponding to an initial energy of ~2.25 GeV. We used an Al-degrader of ~60 μm thick in order to reduce the energy of the impacting ions to ~780 MeV at the apatite-surface. This allows us to reduce the ion penetration depth and associated length of ion-tracks in the apatite to values suitable for confined FT revelation (Jonckheere et al., 2007). The resulting ion range was calculated using the SRIM-software (Ziegler et al., 1985) and yielded ~34 μm. More details on this procedure can be found in Jonckheere et al. (2007) and Min et al. (2007). Thermal history modeling using the HeFTy software (Ketcham, 2005) and the Ketcham et al. (2007) annealing-equations was performed on the two samples that yielded sufficient numbers of track lengths (AI-40 and KYR-13). Default settings of the HeFTy package were retained, except for the l_o-value where 16.05 μm was used as constant and fixed value following our own, laboratory specific induced confined track length calibration.

Samples KYR-06, KYR-07, KYR-12, AI-37 and AI-38 were dated using AFT LA-ICP-MS. The reason why these samples were dated by ICP-MS are purely practical and are associated with the fact that by the time latter samples were prepared for analysis our advances in using AFT LA-ICP-MS at our institute were proving successful. As analysis by ICP-MS in this particular case was also faster, we opted to apply this method. Using LA-ICP-MS for AFT dating is a relative new and experimental approach (Hasebe et al., 2004) and merits and necessitates a somewhat more elaborate description of analytical procedures. In this approach parental ^{238}U concentrations are determined directly by ICP-MS. In the traditional ED method, this is done indirectly by irradiating the samples with thermal neutrons (e.g. Wagner and Van den haute, 1992). This induces ^{235}U fission tracks in the sample and in the contact surface of the muscovite ED in contact with the sample. Counting of the induced tracks gives a measure of ^{235}U concentration, which can be translated to ^{238}U concentrations as both isotopes in nature occur in constant ratio of 7.2527×10^{-3} (Steiger and Jäger, 1977). As irradiation facilities containing well-thermalized channels are becoming more scarce, and as irradiated materials and their transport poses specific risks and problems, ICP-MS analyses are proving a promising alternative (Hasebe et al., 2004).

For the ICP-MS approach, aforementioned samples were embedded in epoxy and polished in exactly the same manner as done for the ED method. However, while for the ED method each sample is individually embedded and a separate muscovite ED is attached to each mount, the mounts for AFT LA-ICP-MS dating are made larger (2.5 cm diameter) and thicker (~1 cm) to fit exactly in the ablation cell. Several samples can hence be included in a single mount (row by row) as is usually done for LA-ICP-MS or SHRIMP ZUPb dating. A prismatic section of a single crystal of the Durango apatite age standard was co-embedded with each

Author's personal copy

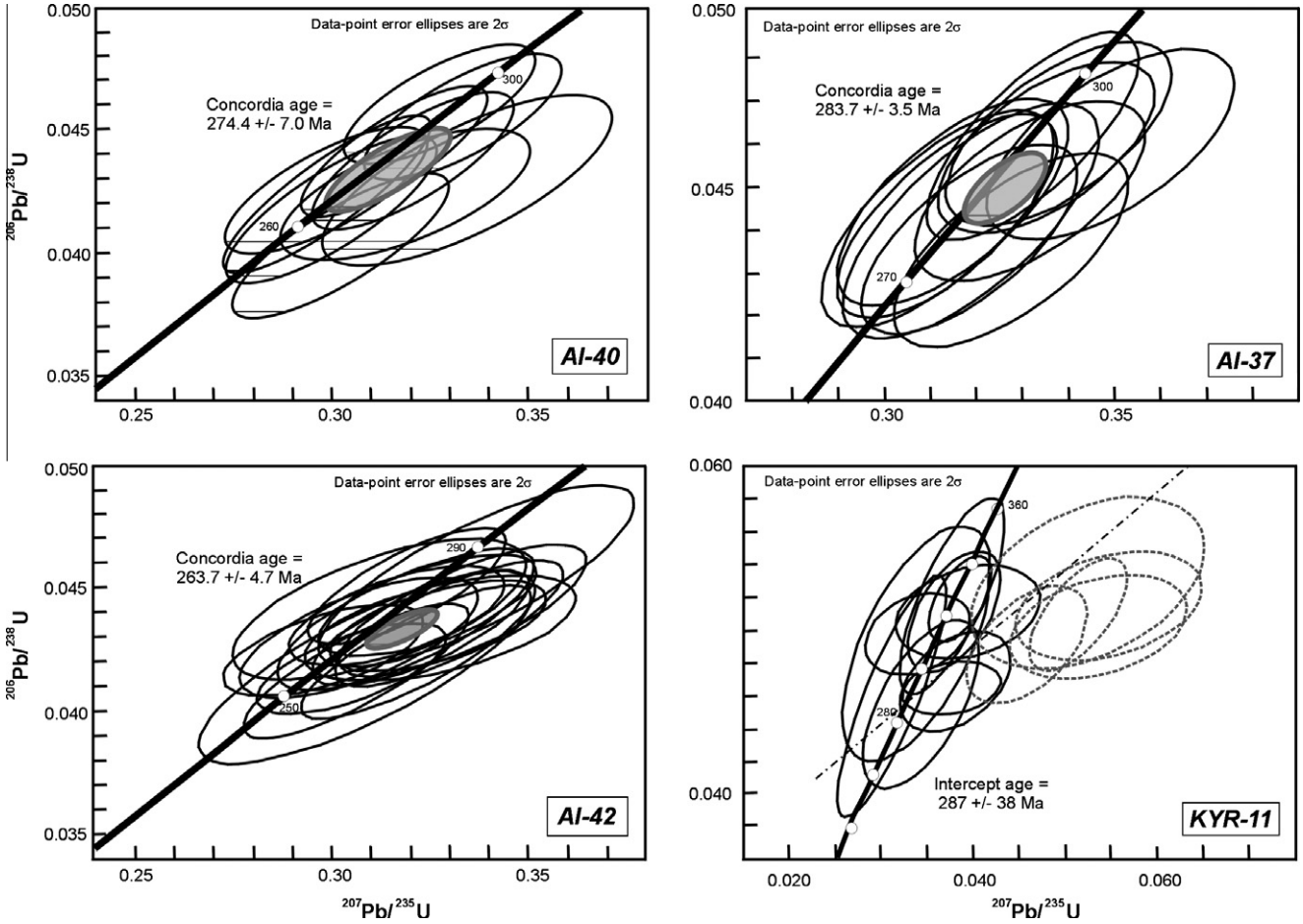

Fig. 4. Concordia plots for zircon U/Pb dating by LA-ICP-MS for samples AI-37, AI-40, AI-42 and KYR-11. The dashed ellipses for KYR-11 represent analyses affected by Pb-loss.

Table 4
AFT age and length data: ρ_s, ρ_i, and ρ_d are the density of spontaneous, induced tracks and induced tracks in an external detector (ED) irradiated against a dosimeter glass. The ρ_d-values are interpolated values from regularly spaced glass dosimeters (IRMM-540). Track densities are all expressed as 10^5 tracks/cm^2. N_s, N_i, and N_d are the number of counted spontaneous, induced tracks and induced tracks in the ED. N_d is also an interpolated value. $P(\chi^2)$ is the chi-squared probability that the dated grains have a constant ρ_s/ρ_i-ratio. An ζ-value of 253.1 ± 2.4 a cm^2 was used for the calculation of $t(\zeta)$, reported in Ma. AFT length data are reported as a mean track length (l_m) with standard deviation σ, obtained from the measurement of a number (n_l) of natural, horizontal confined tracks. For samples indicated by (∗) heavy ion irradiation was used to enhance the number of measurable horizontal confined tracks.

Sample	n	ρ_s (±1σ)	N_s	ρ_i (±1σ)	N_i	ρ_d (±1σ)	N_d	ρ_s/ρ_i	$P(\chi^2)$	$t(\zeta)$	l_m	n_l	σ
KYR-10	20	1.684 (0.133)	161	5.649 (0.243)	539	4.211 (0.081)	2702	0.298 ± 0.027	1.00	15.9 ± 1.5	–	–	–
KYR-13	30	32.851 (0.082)	1617	11.369 (0.048)	567	3.122 (0.080)	1848	3.008 ± 0.147	0.29	117.8 ± 6.5	12.64	100	1.23
AI-40∗	100	2.407 (0.074)	1066	13.370 (0.172)	6061	3.772 (0.076)	2452	0.176 ± 0.006	0.92	8.4 ± 0.3	14.00	40	1.18
AI-42	50	2.660 (0.100)	703	5.975 (0.149)	1595	3.774 (0.076)	2484	0.467 ± 0.021	0.45	22.3 ± 1.1	–	–	–

mount, as well as a row of SH-3 apatite, an "in-house standard" that we use for secondary, internal calibration. SH-3 is a slowly cooled diorite from the Siberian Altai basement (De Grave et al., 2008a) that contains large amounts of exceptionally good apatite grains. The SH-3 sample was dated with the traditional AFT-ED method at 93.1 ± 3.5 Ma using ζ-calibration and at 91.7 ± 3.4 Ma using absolute thermal neutron fluence dosimetry calibration (De Grave et al., 2009; De Grave and Van den haute, 2002). These mounts, containing several apatite samples and standards were then etched to reveal the spontaneous fission tracks, using the same etching conditions as given above for the ED method. The mounts were mapped under a high-resolution zoom-stereomicroscope (Leica M16FA) equipped with a Colorview-I® digital camera (and AnalySIS® software). Spontaneous tracks were counted under a BH-2 microscope (1250 × magnification, dry objectives) using a calibrated micrometer grid of 60 μm by 60 μm. Micro-photographs of the grains were used to indicate the exact position of the counted surface. These exact same 60 μm by 60 μm surfaces were then analyzed for ^{238}U content by LA-ICP-MS using operational conditions listed in Table 2. The LA-ICP-MS instrumental set-up is identical as for the U/Pb measurements, described earlier.

LA-ICP-MS AFT ages were calculated following the method described by Hasebe et al. (2004) for a large extent, although some minor adaptations were made as outlined below. For each measurement (run), the ^{238}U signal intensity was calibrated against ^{44}Ca (internal standard), which is present in both the standards and the unknowns (apatite) as a matrix element. Calibration was performed using NIST 610 and NIST 612 glasses as primary standards, which were measured interspaced between 10 unknown apatite grains within one sequence. The resulting calibration lines are shown in Fig. 5. The origin of the deviate signal sensitivity for sequence 3 and 4 versus sequence 1 and 2 is unclear but has no effect on the calculated U-concentration due to the repeated measurements of NIST-standards within each sequence. This was

Author's personal copy

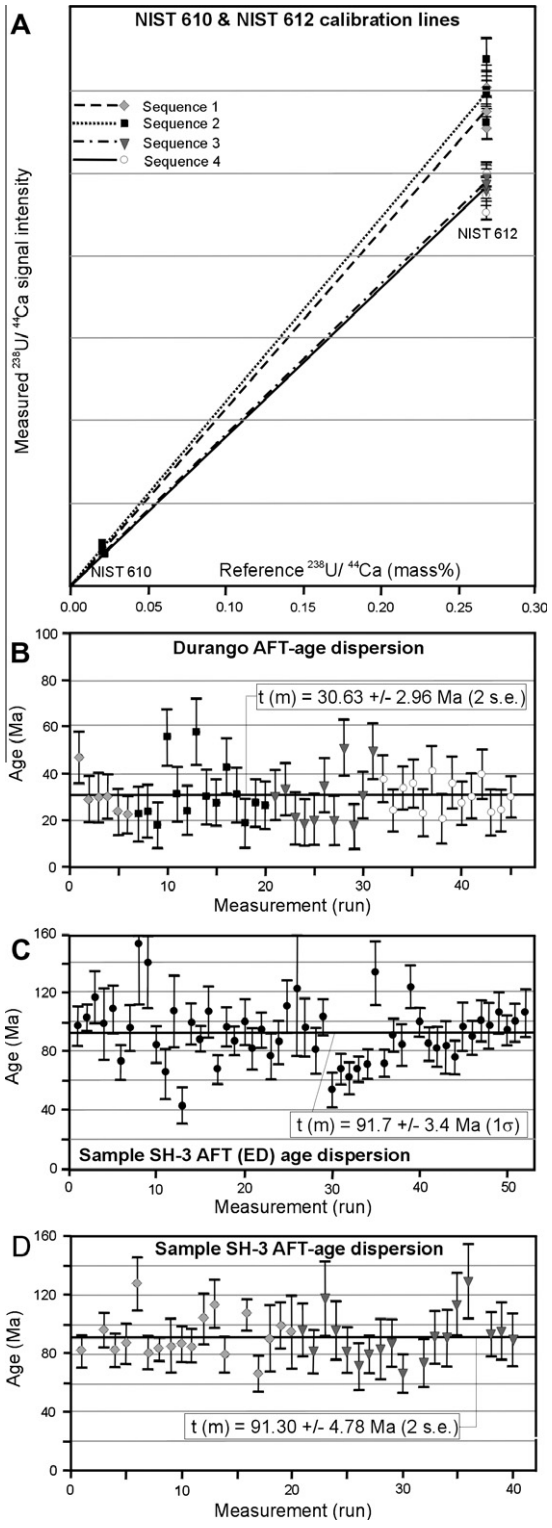

Fig. 5. (A) The LA-ICP-MS $^{238}U/^{44}Ca$ signal intensity was calibrated against NIST 610 and 612 glass standards (Jochum and Stoll, 2008), following the method described in Hasebe et al. (2004). The deviate sensitivity for sequence 1 and 2 versus sequence 3 and 4 is unclear but has no effect on the resulting LA-ICP-MS AFT ages. (B) Accuracy check of the resulting ages was performed using the Durango apatite age standard. The mean age of 30.63 ± 2.96 Ma (2SE) is in good agreement with the reference age of 31.44 ± 0.09 Ma (McDowell et al., 2005). Symbols as in (A). (C). Sample SH-3 was also measured as an independent check of the accuracy. Symbols as in (A). This slower cooled basement sample (De Grave et al., 2009) yields an AFT age (using the conventional method – absolute, i.e. non-zeta approach) of 91.7 ± 3.4 Ma (1σ). (D) The mean LA-ICP-MS AFT age was calculated as 91.30 ± 4.78 Ma (2SE) which is in excellent agreement with the AFT age obtained using the conventional method as shown in (C).

controlled using two secondary standards (accuracy check): Durango apatite and the SH-3 apatite as explained above (Fig. 5). Although negligible, within-sequence instrumental drift-correction was performed based on the NIST 612 $^{238}U/^{44}Ca$ output. The CaO-content is well-known for the NIST and Durango-standards (GEOREM preferred values – Jochum and Stoll, 2008; Seifert et al., 2000). For SH-3 and the unknown apatite samples, CaO-content was measured using SEM-EDX (JEOL JSM-6400) and calibrated against Durango apatite (CaO measured: 55.7 ± 0.8 wt.% (1σ); CaO reference: 54.0 ± 0.2 wt.% (1σ), Seifert et al., 2000; Table 5).

The LA-ICP-MS AFT ages were calculated using an absolute approach, which is based on the ^{238}U total decay constant and the ^{238}U spontaneous fission-decay constant. Therefore, the age-equation of Hasebe et al. (2004) was used,

$$t = \frac{1}{\lambda_D} \ln\left(1 + \frac{\rho_S \lambda_D M}{\lambda_f N_A^{238} U 10^{-6} d R_{sp} k}\right) \quad (1)$$

where λ_D = ^{238}U total decay constant (1.55125×10^{-10} a^{-1}, Jaffey et al., 1971), λ_f = ^{238}U spontaneous fission-decay constant (8.46×10^{-17} a^{-1}, Galliker et al., 1970; Wagner and Van den haute, 1992), N_A = Avogadro's number (6.02214×10^{23} mol^{-1}), d = apatite density (3.19 g/cm^2 as in Hasebe et al., 2004), M = the atomic mass of ^{238}U (238.0508 amu), k = observational parameter = 1 are constants. ^{238}U is the measured 238-Uranium concentration (in μg/g) in the sample, ρ_s is the spontaneous fission track density (in tracks/cm^2) and R_{sp} is a registration factor, and corresponds to the range or to half of the measured mean confined fission-track length. The total uncertainty on this age (for each analyzed grain) is given by (Hasebe et al., 2004):

$$\text{age uncertainty} = t\sqrt{\left(\frac{1}{N_S^2} + \delta^2\right)} \quad (2)$$

where t = the calculated AFT age, N_s = the number of counted spontaneous fission tracks, δ = total uncertainty in ^{238}U concentration (propagated uncertainty, generally 5–10%). The results are reported in Table 5.

In our calculations, we used R_{sp} = 7.25 for the Durango apatite age standard, which is half of the average mean confined FT length for fossil tracks in this standard ($l_m \sim 14.5$ μm; Jonckheere et al., 2007; Glorie et al., 2010b). For sample SH-3, half of the actually measured mean confined FT length of 6.6 μm was used (De Grave et al., 2009). In samples AI-37 and AI-38, the number of confined tracks was not sufficient and no sample specific R_{sp}-value could be measured. We therefore used R_{sp} = 7.05 μm, which is the measured mean confined FT length for sample AI-40, a rapidly cooled basement sample with a similar AFT age (and thermal history) and a similar crystallization age and lithology. For the detrital apatite samples from the southern edge of the Alai Valley (KYR-06; KYR-07), several age components could be identified. We used RadialPlotter (Vermeesch, 2009) to visualize the different components and calculated a central age for each age-group (Fig. 6). Although the number of analyzed grains is relatively low for these sedimentary samples due to reasons of apatite grain quality, three major age components could be distinguished for both samples, while an additional younger component for KYR-06 was found as well. For these samples, R_{sp} = 7.05 μm was used, the value for the fast cooled basement samples. We are aware that this might introduce a small bias in the age of the age components that cooled slower, which is possibly the case for the Cretaceous components. In theory, these ages can hence be seen as minimum ages, with the true AFT age being 10% older at most. Given the cooling ages and modeled tT paths for the Cretaceous KYR-13 sample (Fig. 7) however, we are confident that the R_{sp} values adopted here do not introduce significant errors.

Author's personal copy

Table 5
ρ_s is the surface density of spontaneous fission tracks (in 10^5 tracks/cm^2). N_s is the number of counted spontaneous tracks, and n is the number of counted grains. ^{238}U is the average ^{238}U concentration, measured by LA-ICP-MS (in μg/g), CaO the average CaO concentration, measured by SEM-EDX (mean value in wt.%; here reported as uncorrected values). The AFT age (t) is given in Ma and was calculated by using the Hasebe et al. (2004) equation, see text for additional details.

Sample	ρ_s	1σ	N_s	n	^{238}U	1σ	CaO	1σ	t (Ma)	1σ
AI-37	1.759	0.139	160	30	26.84	1.87	55.2	0.6	18.8	1.6
AI-38	2.177	0.155	198	30	35.46	3.49	55.4	1.3	14.0	1.4
Kyr-06_A	5.102	0.736	48	3	5.45	0.55	55.0	0.4	206.6	12.2
Kyr-06_B	2.232	0.344	42	6	6.26	1.02	55.0	0.4	71.8	6.8
Kyr-06_C	2.372	0.217	119	16	25.78	9.52	55.0	0.4	18.4	1.7
Kyr-06_D	0.850	0.301	8	3	52.37	7.76	55.0	0.4	3.3	0.7
Kyr-07_A	11.161	0.545	420	12	11.72	0.94	55.4	1.5	208.0	16.6
Kyr-07_B	8.503	0.549	240	9	21.28	2.27	55.4	1.5	80.7	7.0
Kyr-07_C	2.934	0.433	46	5	35.55	3.03	55.4	1.5	18.9	3.1
Kyr-12	3.968	0.399	99	8	3.58	0.51	55.7	0.5	223.0	19.3

2.3. Apatite (U–Th–Sm)/He thermochronology

The apatite (U–Th–Sm)/He (AHe) method is even more sensitive to low-temperature perturbations (order of magnitude ~40–80 °C) than the AFT technique and is thus a more sensitive thermochronometer. It is based on the diffusion of radiogenic ^{4}He through the crystal lattice at elevated temperatures (Stockli et al., 2000; Ehlers and Farley, 2003) and it is an ideally suited complementary technique to AFT.

While sample preparation was carried out in our facilities, He analysis was performed at the (U–Th)/He laboratory of Kansas State University (USA) and analytical procedures are described in detail e.g. by Farley and Stockli (2002). Apatite grains were selected under a high-resolution zoom-stereomicroscope equipped with polarized light to exclude even the smallest inclusions. The three most ideally suited grains (no inclusions, transparent, euhedrical hexagonal prisms) were loaded in separate platinum sleeves (Pt tubes). Each grain is photographed and the crystal's dimensions were determined to allow for α-ejection correction based on the F_T ejection correction method (Farley, 2002; Farley et al., 1996). Sample aliquots in the Pt sleeves were heated by a 20 W Nd-YAG laser (House et al., 2000) to fuse the grains in the Pt and evacuate the ^{4}He gas from the mineral lattice. The ^{4}He was measured by isotope dilution (^{3}He spike), after gettering and cryogenic purification, with a Blazers Prisma QMS-200 quadrupole mass spectrometer. After dissolution, U, Th and Sm concentrations were determined by a VG Plasmaquad-2 ICP-MS. Results for the AHe analyses are listed in Table 6, and ages are ploted on the map in Fig. 3.

3. Results

3.1. Zircon U/Pb dating

Zircon U/Pb dating results are presented in Table 3 and corresponding Concordia plots and age results are presented in Fig. 5. Ages are also indicated on the map in Fig. 3. The granites in the northern-central part of the Alai Range (Kokbulak Mountains, Belauli and Askaly bodies) yield a zircon U/Pb age of 283.7 ± 3.5 Ma (sample AI-37). This zircon crystallization age suggests that the granites were emplaced in the Early to Middle Permian. Sample KYR-11 from the amphibolitic contact aureole of the Belauli and Askaly plutons does not exhibit a clear concordant age. Pb-loss during the thermal metamorphic event might be responsible for this shift from Concordia. A lower intercept age of 287 ± 38 Ma could be deduced from this data. This coincides with the granite crystallization age of AI-37 and constrains the thermal metamorphic event.

Samples AI-40 and AI-42 from the granites in the southern part of the Alai Range, from the Dzhaman-Dzhailiuski, Sary-Mogol and Balyktinski intrusions have a somewhat younger age with respect to AI-37. Concordant zircon crystallization ages were found to be 274.4 ± 7.0 Ma (AI-40) and 263.7 ± 4.7 Ma (AI-42), corresponding to a Middle Permian (Guadalupian) formation of these intrusives.

3.2. Apatite fission-track thermochronology

Results from AFT dating and length measurement can best be described in three groups. A first group only contains a single sample, KYR-13. This sample is a Late Carboniferous–Permian conglomerate (Fig. 3) from a molasse unit containing granitic clasts, presumably from the Permian granites in the vicinity. The sample (including granitic clasts and sandy matrix) was dated by the traditional AFT-ED method and gave an apparent mean Early Cretaceous AFT age of 117.8 ± 6.5 Ma. The length distribution for this sample produces a mean length of 12.64 μm, with standard deviation of 1.23 μm (Fig. 7, Table 4). These values suggest a relatively long residence time in the Apatite Partial Annealing Zone (Wagner and Van den haute, 1992) and are typical for slowly cooled basement rocks (Gleadow et al., 1986). The Early Cretaceous apparent AFT age of the sample can hence be interpreted as a cooling age through APAZ temperatures. This further suggests that between deposition in the Late Carboniferous–Permian and cooling in the Early Cretaceous, the sample was heated to temperatures exceeding partial annealing conditions, i.e. temperatures in excess of 110–120 °C. The extent of heating was sufficient to reset all apatites (from the granitic clasts as well as from the matrix), resulting in the complete annealing of the pre-Early Cretaceous signal. The most plausible explanation for this observation is that the Late Carboniferous–Permian molasse unit was buried by Early and Middle Mesozoic sediments to the extent sedimentary load reached a threshold whereafter complete resetting of the AFT "clock" could occur (burial induced heating). After this, from a thermochronology viewpoint, this sample can be considered as a "basement" sample with its specific Late Mesozoic to recent cooling history. Early Cretaceous denudation of the Early and Middle Mesozoic overburden would then have exhumed the sample and brought it back in APAZ temperatures. The fact that the AFT lengths have a unimodal distribution and clearly show shortening, implies that the Early Cretaceous event was insufficient to bring the sample completely to the (sub)surface and that it was subjected to partial annealing for a non-negligible amount of time. This qualitative description is reflected in the thermal history model for this sample (Fig. 7): after Early to Middle Mesozoic total annealing, an Early Cretaceous event between ~140 and 110 Ma places the Late Carboniferous–Permian conglomerate back in the APAZ. After a period of Late Cretaceous–Early Cenozoic stability, a Late Cenozoic cooling event is ultimately responsible for final cooling of the conglomerate to present outcrop temperatures. Initiation of this latest "basement" cooling is modeled at ~15–20 Ma (Fig. 7). This corresponds to the denudation of the modern Tien Shan orogen and is underscored by the basement cooling ages obtained in this study (see below).

Author's personal copy

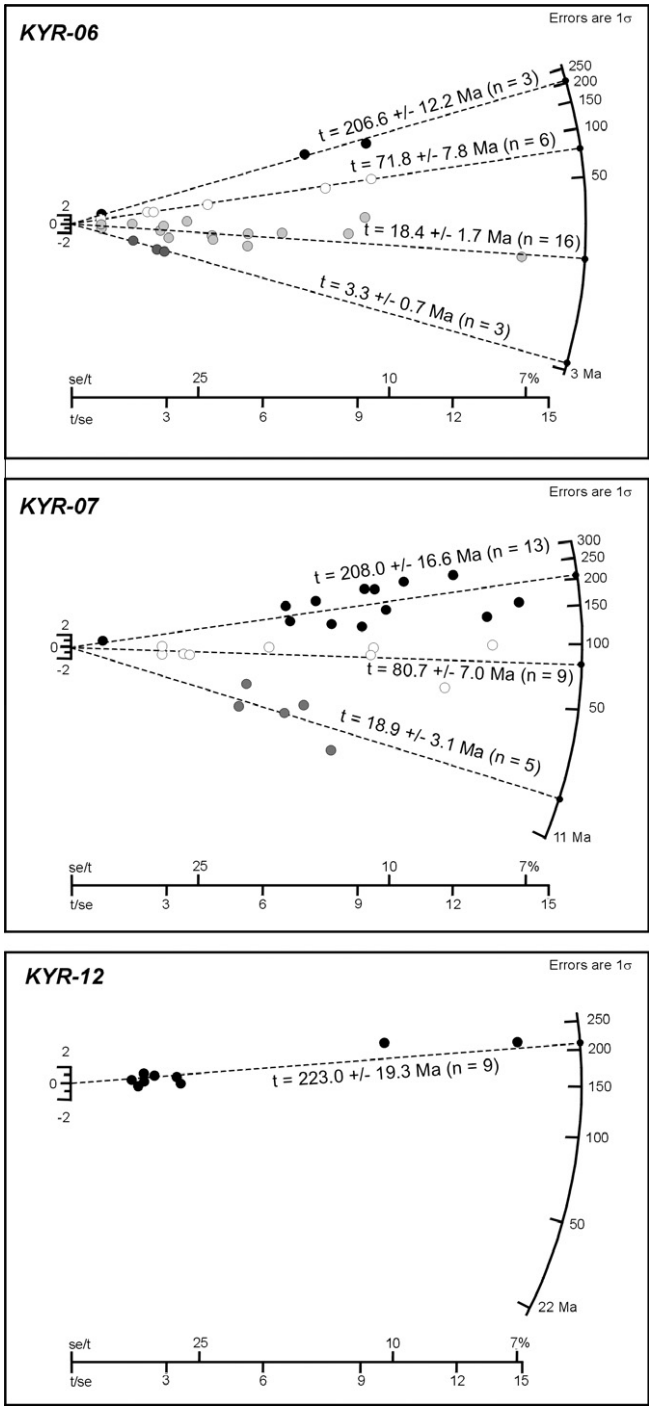

Fig. 6. Radial plots showing age components of the detrital apatite samples from the Trans-Alai foreland (KYR-06 and KYR-07) and the Ferghana Basin (KYR-12). See text for discussion. Plots made using the RadialPlotter software (Vermeesch, 2009).

A second group of samples is represented by detrital apatites from sandstones originating from both the southeastern Ferghana Basin (sample KYR-12) and the Alai Basin and Trans Alai Range (samples KYR-06 and KYR-07). These basins border the current Alai (and Kichi-Alai) Ranges to the north and south respectively. All samples from this group were dated using AFT LA-ICP-MS. Although care was taken to extract as many good quality apatites as possible, the amount of datable grains was not always high. Nevertheless several age populations (central ages) could clearly be distinguished in the detrital samples (Fig. 6, Table 5). Sample KYR-12, a Cretaceous sandstone from the southeastern Ferghana Basin (Fig. 8) only shows one age population of 223.0 ± 19.3 Ma. As a "reset" Triassic age due to burial and heating for the Cretaceous sandstone is obviously not possible, the sandstone hence contains non-reset detrital apatites from a source region that apparently cooled in the Late Triassic (Carnian). A Late Triassic age component was also found for the Trans-Alai samples (Fig. 6), however, the ages are somewhat younger than for the Ferghana Basin sample: 208.0 ± 16.6 Ma (KYR-07) and 206.6 ± 12.2 Ma (KYR-06) (Norian). Both Trans-Alai samples subsequently contain a Late Cretaceous (Campanian) age component of 80.7 ± 7.0 Ma (KYR-07) and 71.8 ± 7.8 Ma (KYR-06). An Early Miocene (Burdigalian) component of 18.9 ± 3.1 Ma (KYR-07) and 18.4 ± 1.7 Ma (KYR-06) is also recognized in both samples. An even younger, Late Pliocene age population of 3.3 ± 0.7 Ma is only found in sample KYR-06. Sample KYR-07 represents the basal units of the Neogene Trans-Alai sediments, and was sampled close to the Oligocene outcrops (Fig. 8). KYR-06 was taken from the upper Neogene section and not-surprisingly therefore is the only sample hosting the youngest age population. Samples KYR-07 and KYR-06 correlate to the Late Oligocene–Middle Miocene Massaget Complex and the Middle Miocene–Pliocene Baktry Formation in the Central Alai Valley respectively (Coutand et al., 2002). The aforementioned age components preserved in the detrital record are also found in several localities within the Tien Shan basement rocks (e.g. De Grave et al., 2008b) were they appear to pinpoint several cooling events affecting the Tien Shan basement during Meso-Cenozoic reactivation episodes. However the age components for these three samples might also in part represent mixed ages. Without track length data this cannot be ruled out. Given the limited amount of datable grains, insufficient amount of confined tracks were found for these samples.

Finally, a third group is represented by granitic basement rocks from the northern-central Alai Range (Kokbulak Mountains, Belauli and Askaly plutons, samples KYR-10, AI-37 and AI-38) and the southern Alai Range (Dzhaman-Dzhailiuski, Sary-Mogol and Balyktinski intrusions, samples AI-40, AI-41, and AI-42). Samples AI-37 and AI-38 were dated with the AFT LA-ICP-MS method (Table 5), while for the other three, the more traditional ED method was applied (Table 4). All these granite samples render young AFT ages (Fig. 3) and low spontaneous track densities. No clear AFT age – elevation trends could be observed. Only for sample AI-40, which contained the most and best-quality apatite grains, enough grains were present to allow a significant track length measurement and thermal history modeling (Fig. 7). Even so, confined track densities had to be enhanced by using heavy-ion bombardment and only 40 lengths could be measured. All AFT ages are Early Miocene with 18.8 ± 1.6 Ma (AI-37), 15.9 ± 1.5 Ma (KYR-10) and 14.0 ± 1.4 Ma (AI-38) in the north, and Early to Late Miocene with 22.3 ± 1.1 Ma (AI-42) and 8.4 ± 0.3 Ma (AI-40) in the south of the Alai Range. The mean track length for AI-40 is 14.00 μm with a standard deviation of 1.18 μm, suggestive of a rapid and recent cooling. When performing thermal history modeling the young AFT age and long AFT track lengths (with added AHe – input) not surprisingly produce an envelope of good fit tT paths that pass the APAZ rapidly during the past ~10 Ma. The Miocene ages for the granitic basement correspond to the Miocene age components in the detrital samples (group 2, above) and to the modelled Late Cenozoic cooling for the Early Cretaceous sample KYR-13 (group 1, above). All these point to an Early Miocene onset of denudation of the Kyrgyz Southern Tien Shan and the leading edge of the advancing Pamir thrust nappes.

3.3. Apatite (U–Th–Sm)/He thermochronology

For the southern Alai Range samples from the Dzhaman-Dzhailiuski, Sary-Mogol and Balyktinski intrusions (AI-40, AI-41, and

Author's personal copy

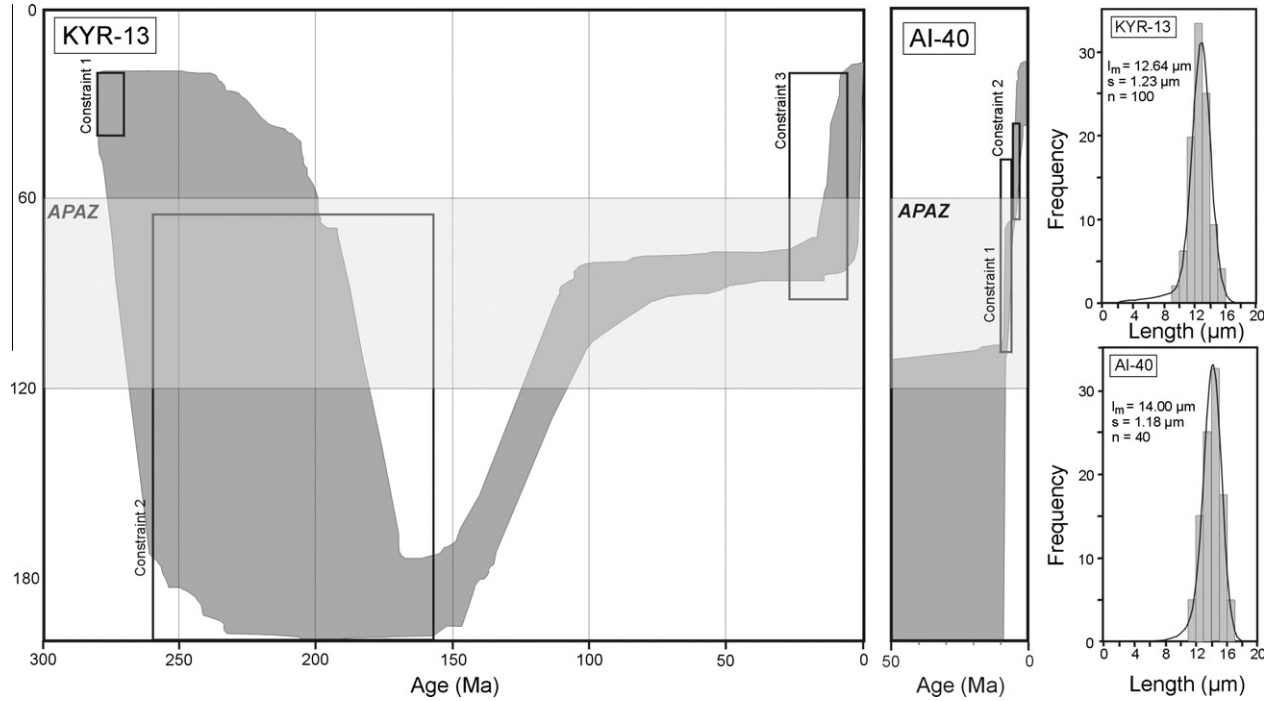

Fig. 7. Thermal history models of representative samples: KYR-13 is a Carboniferous–Permian conglomerate sample at the Alai Range–Ferghana Basin transition. AI-40 is a granite sample that represents the recently cooled basement, linked to Late Cenozoic denudation of the modern Tien Shan orogen. Length distributions are also shown. Thermal history modeling was performed using the HeFTy software (Ketcham, 2005) and Ketcham et al. (2007) annealing-equations. AI-40 data contains both AFT and He input. Only the envelope of "good" tT paths is shown, "acceptable" fits are left out. APAZ = Apatite Partial Annealing Zone. Constraints were placed based on geological arguments. For KYR-13, constraint 1 = depositional age at (sub)surface temperatures; constraint 2 = Mesozoic burial, Mesozoic sediments from the Ferghana Basin push the sampled rocks back in and through the APAZ and reset the AFT "clock" before Late Mesozoic exhumation; constraint 3 = Late Cenozoic denudation as evidenced by basement cooling and detrital apatites. For AI-40, constraint 1 = AFT age suggest passing of the APAZ; constraint 2 = suggests passing through AHe closure temperature range. A third, high-temperature constraint for AI-40, is far outside the scale of the Fig. and represents the Permian emplacement of the pluton (zircon U/Pb age of ~275 Ma). No *c*-axis projection was used for modeling because our etching conditions show a deviate trend from the used models (Glorie et al., 2010b). Default settings were retained, except for the l_o-value where 16.05 µm was used as constant and fixed value following our own, laboratory specific induced confined track length calibration.

Table 6
Apatite (U–Th–Sm)/He dating results. Aqt = Aliquot number. Concentrations for U, Th and Sm are listed in ppm, the ^{4}He concentration is in ncc/µg. The mass, *m*, of the apatite grains is in µg. F_T is the ejection correction factor. Single grain ages for each aliquot are given, and an average sample value is calculated. For comparison, where available, AFT ages are listed as well. Two AI-41 aliquots were rejected, see text.

Sample	Aqt	U	Th	Sm	Th/U	He	*m*	F_T	Age	Average	AFT age
AI-40	1	4.2	9.6	12.5	2.3	0.11	3.2	0.69	4.5 ± 0.3		
	2	4.0	8.8	12.3	2.2	0.11	2.3	0.66	5.1 ± 0.3		
	3	1.7	3.2	6.3	1.9	0.05	13.5	0.80	5.4 ± 0.4	5.0 ± 0.3	8.4 ± 0.3
AI-41	1[a]	1.7	2.1	5.7	1.2	*0.00*	4.7	0.72	–		
	2[a]	0.9	2.2	7.8	2.3	*11.57*	4.0	0.71	–		
	3	2.5	4.1	16.0	1.6	0.16	2.6	0.67	12.5 ± 0.8	12.5 ± 0.8	–
AI-42	1	0.7	1.0	1.8	1.3	0.04	31.2	0.85	8.5 ± 0.4		
	2	25.7	32.7	68.4	1.3	1.20	2.0	0.64	10.2 ± 0.6		
	3	2.0	3.1	6.0	1.5	0.13	18.0	0.82	10.3 ± 0.6	9.7 ± 0.6	22.3 ± 1.1

[a] Rejected.

AI-42), apatite (U–Th–Sm)/He (AHe) ages were obtained as well (Table 6). With respect to the AFT ages, the AHe ages are younger, as the closure temperature of the latter system is lower. The acquired AHe ages are Late Miocene–Early Pliocene and thus further corroborate the Miocene cooling of the Alai crystalline basement during denudation of the growing orogen. AHe analyses were done in triplicate. The three single grain aliquots for samples AI-40 and AI-42 all generated reproducible (F_T corrected) Late Miocene–Early Pliocene ages and yield an average of 5.0 ± 0.3 Ma and 9.7 ± 0.6 Ma respectively. Sample AI-41 did not contain sufficient good quality apatites and its AFT mount did not include datable grains at all. Also the selected AHe grains proved of low quality and two aliquots had to be rejected (Table 5). A first AI-41 aliquot did not release any radiogenic helium gas, while the grain from a second aliquot produced unsupported, parentless ^{4}He, probably originating from undetected and indissolvable U- and/or Th-rich micro-inclusions. A last aliquot however rendered a Late Miocene AHe age of 12.5 ± 0.8 Ma that fits nicely with both other AHe ages and hence, while only from one aliquot, it is considered to be a reliable age.

4. Interpretation and discussion

4.1. Zircon U/Pb data

The geochronologic and thermochronologic data presented here pinpoint several events in the tectonic evolution of the Alai region geology in an absolute timeframe. All ages obtained with the

Author's personal copy

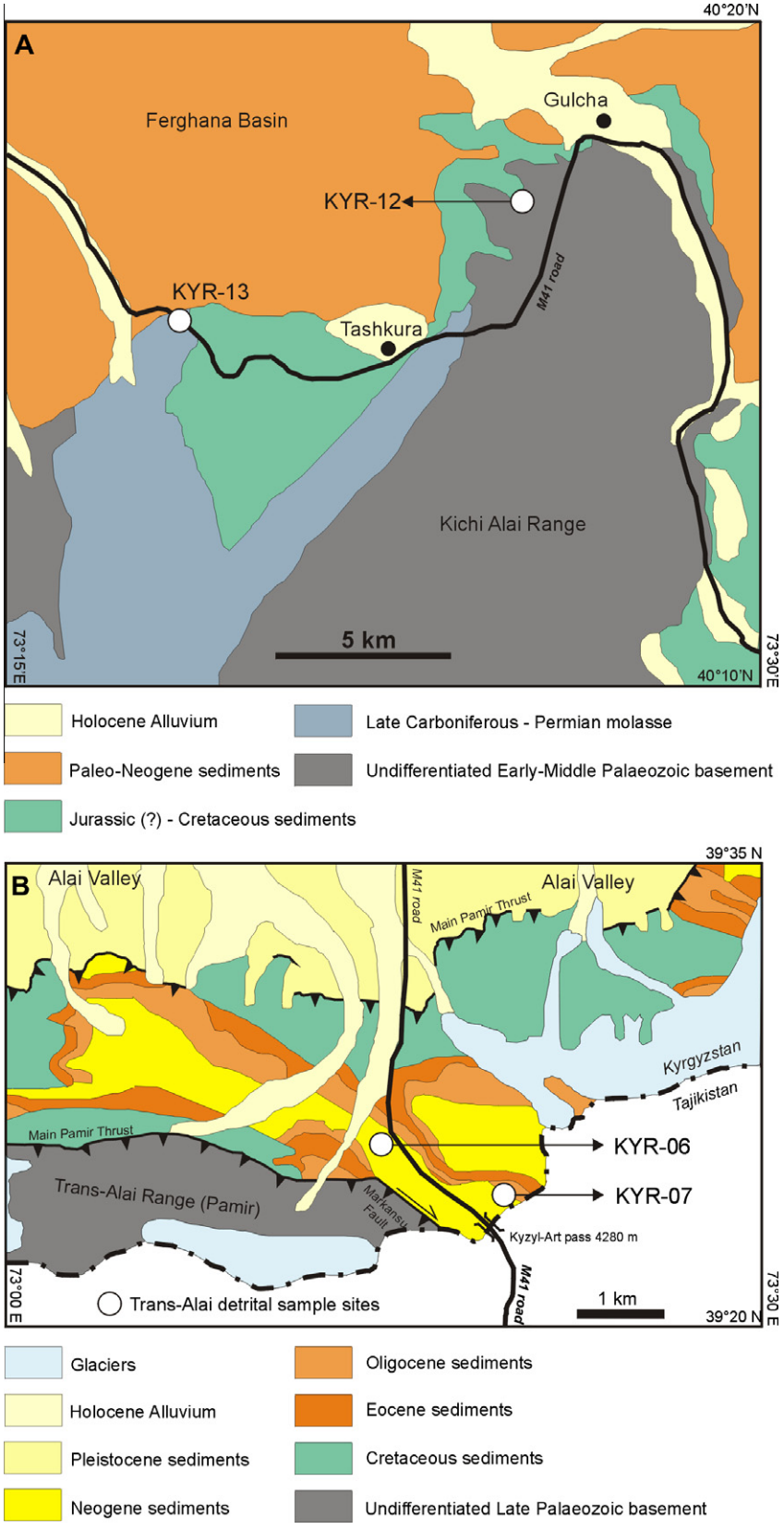

Fig. 8. (A) Detailed geological map of the south Ferghana Basin and the northern Kichi-Alai Range. Sample positions (detrital apatite) for KYR-12 and KYR-13 are indicated. See box in Fig. 3 for overview. (B) Detailed geological map of the south Alai Valley and the Trans-Alai Range, Pamir transition. Sample positions (detrital apatite) for KYR-06 and KYR-07 are indicated. See box in Fig. 3 for overview. Maps based on Tursungaziev and Petrov (2008) and schematic structures for the south Alai Valley and the Trans-Alai Range from Strecker et al. (2003).

various techniques are schematically shown in Fig. 9A and span the Late Palaeozoic to the present. A first age signal is represented by the Early to Middle Permian emplacement ages of the granitic intrusion in the Alai region of the STS. In the northern-central part

Author's personal copy

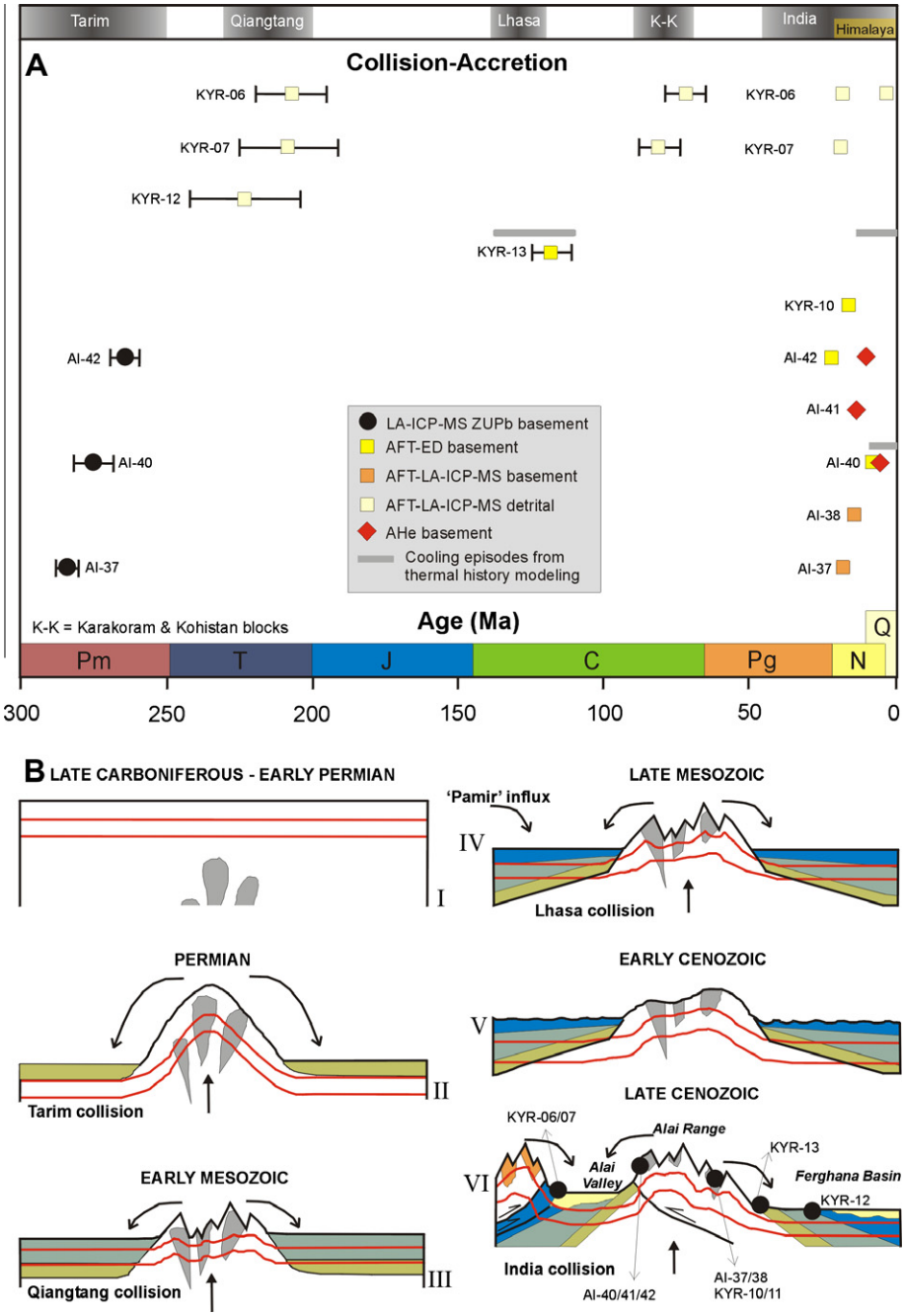

Fig. 9. (A) Tectonic events associated to the ages obtained for the Alai and Trans-Alai samples from multi-method geochronology and thermochronology. Time is shown in abscissa, *Y*-axis is arbitrary and dimensionless and solely differentiates between the samples. Abbreviations: AFT = Apatite Fission Track dating, AHe = Apatite (U–Th–Sm)/He dating, ED = External Detector method, LA-ICP-MS = Laser Ablation-Inductively Coupled-Mass Spectrometry, ZUPb = Zircon U/Pb dating. See text for discussion. (B) Cartoon schematically showing the tectonic evolution of the Alai region. Red lines represent the ~60 °C and 120 °C isotherms (AFT sensitivity). (I–II) In the Late Carboniferous–Early Permian, Tarim collided with palaeo-Kazakhstan introducing post-collisional granitoids and causing basement uplift and erosion with deposition of Late Carboniferous–Permian molasse units. (III) Collision of Qiangtang reactivated the Tien Shan and associated denudation resulted in thick Early Mesozoic deposits. Due to this burial, Permian sediments were heated above 120 °C, erasing the pre-Triassic AFT signal. (IV) In the Late Mesozoic, collision of the Lhasa-block again caused reactivation and produced Late Mesozoic basement cooling and contemporaneous sediments. (V) In the Late Mesozoic–Early Cenozoic, the topography was flattened, and an erosion surface with characteristic red-bed developed. (VI) The indentation of India and the Pamir promontory in Eurasia eventually built the modern Tien Shan orogen and the present-day Alai Range as distal effects. Associated uplift and denudation occurred in a punctuated fashion, starting the Early Miocene, with intensification in the Early Pliocene, and continuing today. Sample sites are schematically indicated.

of the Alai Range (Kokbulak Mountains, Belauli and Askaly bodies) we find an Early Permian emplacement and associated thermal metamorphism of ~285 Ma. In the southern part of the Alai Range (Dzhaman-Dzhailiuski, Sary-Mogol and Balyktinski intrusions) a somewhat younger age of ~274–264 Ma is found, corresponding to the Middle Permian Guadalupian Epoch. These Permian ages correspond to a well-known episode of post-collisional magmatism of which signs are ubiquitous throughout the entire Tien Shan orogen. The post-collisional granitoids appear in all composing tectonic units of the Tien Shan and hence their intrusion occurred when the ancestral Tien Shan was amalgamated completely. The ages found in the Alai segment and reported in this paper,

Author's personal copy

especially the older ones of ~285 Ma, correspond well with ages published for the Kokshaal segment of the Kyrgyz STS (Konopelko et al., 2007, 2009; Seltmann et al., in press). These authors report (mainly SHRIMP) zircon U/Pb ages between about 299 and 279 Ma. Rb/Sr isochron ages of 275–269 Ma from the Kokshaal plutons are reported by Solomovich and Trifonov (2002). For the Kyzylkum segment of the STS, Seltmann et al. 2011 give an overview of Early Permian post-collisional magmatism with emplacement ages of 293–276 Ma. In the Middle Tien Shan ages for the Permian post-collisional magmatism range from about 294 to 279 Ma (Alekseev et al., 2009; Konopelko et al., 2009; Seltmann et al., 2011). In the Kyrgyz Northern Tien Shan ages of 292 Ma are found (Glorie et al., 2010a; Seltmann et al., 2011). In the Chinese part of the Southern Tien Shan, Long et al. (2008) and Gao et al. (2009) report ages of 285–280 Ma for post-collisional igneous complexes there and Wang et al. (2009a,b; and references therein) report Permian intrusion ages of about 290–260 Ma in the Northern and Central Chinese Tien Shan. Many of these "Hercynian" post-collisional granitoids are associated with important ore deposits (mainly Au) that have been dated to the Early Permian, ranging roughly between 280 and 290 Ma (Mao et al., 2004; Morelli et al., 2007). In general our ages from the Alai segment of the Kyrgyz STS of ~285–264 are within the youngest range, or in all, consistently slightly younger than those listed above from the NTS, MTS, Kokshaal segment of STS in Kyrgyzstan and the Chinese STS.

The Permian post-collisional plutons across the Tien Shan are related to the final amalgamation stage of the ancestral Tien Shan orogen and of the CAOB as a whole. The ancestral Tien Shan was constructed when frontal collision of the palaeo-Kazakhstan continent with (Karakum)-Tarim occurred (Allen et al., 1992, 1995; Carroll et al., 1995; Gao et al., 1998; Heubeck, 2001; Windley et al., 2007; Xiao et al., 2010). Next to the development of post-collisional igneous complexes, this large-scale orogenic event produced significant relief in the Tien Shan orogen and thick Permian molasse type deposits accumulated in the foreland and intramontane basins (e.g. Graham et al., 1993). The conglomerate KYR-13 sample comes from such a deposit on the southeastern margin of the Ferghana Basin.

4.2. Apatite low-temperature basement and detrital thermochronology

In the Early Mesozoic (possibly already to some extent in the Middle to Late Permian) the KYR-13 sample was buried under a thick sedimentary sequence. Detrital apatites from a Cretaceous sandstone (KYR-12) from the southeastern Ferghana Basin in the vicinity of the KYR-13 sample site, record sediment influx in the Ferghana Basin from a source area characterized by an apparent Late Triassic AFT cooling age of ~223 Ma. A Late Triassic age component in the Late Cenozoic sediments (KYR-06 and KYR-07) along the Trans-Alai Range is present as well. For the latter samples the Late Triassic ages are a bit younger, around ~207 Ma. In the Tien Shan post-Late Triassic denudation has largely erased this thermochronologic signal from the basement rocks, although in some distinct areas (most notably on the Song-Kul Plateau, Fig. 2, De Grave et al., 2008b), remnant AFT Triassic cooling ages are preserved. Also in distinct parts of the Chinese Tien Shan several authors report Late Triassic AFT cooling ages (Dumitru et al., 2001; Sobel et al., 2006a) although there as well, this age component is rather rare and only present in the detrital record. Far less, if at all, in the basement. In any case, these AFT ages point toward a Late Triassic episode of basement cooling through denudation and subsequent deposition of the eroded sediments. In the region Late Triassic to Early Palaeogene sediments are ubiquitous and form deposits of several kilometers thick in the Ferghana Basin (Burov et al., 1990; Tursungaziev and Petrov, 2008). This episode is contemporaneous with the collision of the Cimmerian ("Tibetan") block of Qiangtang with the then southern (southeastern) (Eur)Asia margin of the evolving Pangean supercontinent along the Jinsha suture south of Tarim (northern Tibet and across the Pamir blocks) (e.g. Yin and Harrison, 2000 and references therein; Schwab et al., 2004). The collision–accretion of Qiangtang resulted in tectonic reactivation in the Tien Shan orogen as seen in the structural geologic, sedimentary and thermochronologic record (e.g. Hendrix et al., 1992; Allen et al., 1993; Graham et al., 1993; Dumitru et al., 2001; Vincent and Allen, 2001). We interpret the Late Triassic detrital AFT age signal (as Late Triassic cooling ages of the source basement) in the southeastern Ferghana Basin and the Trans-Alai as related to this event (Fig. 9).

A next 'signal' detected in our thermochronologic dataset from the Alai area is picked up in the Early Cretaceous (Fig. 9A). A Permian conglomerate from a Late Carboniferous–Permian molasse unit at the Alai Range–Ferghana Basin transition yields an AFT cooling age of ~118 Ma (sample KYR-13). This attests to the fact that Early Mesozoic (and probably also to some extent Late Permian) sediments buried this unit sufficiently deep to cause heating above Apatite Partial Annealing Zone (APAZ) temperatures and to thus erase any pre-existing AFT signal. At that time the apatites in this sample were reset and record subsequent cooling in the Early Cretaceous. Thermal history modeling based on the AFT age and length data of sample KYR-13 (no AHe data available) confirms that the sample was rapidly cooled in the Early Cretaceous between ~140 and 110 Ma (Fig. 7). This predates to some extent the deposition of the Cretaceous sediments from which KYR-12 was sampled. These "KYR-12" sediments are in any case older than the Cenomanian (~100–95 Ma) clays and marls above. Unlike the Late Triassic component, Late Jurassic–Early Cretaceous AFT basement cooling ages and detrital AFT age populations are prevalent throughout the entire Kyrgyz and Chinese Tien Shan (e.g. Sobel and Dumitru, 1997; Bullen et al., 2001; Dumitru et al., 2001; Sobel et al., 2006a,b; De Grave et al., 2008b; Wang et al., 2009a,b; Glorie et al., 2010a; Jolivet et al., 2010). This widespread Late Jurassic–Early Cretaceous event is probably related to the collision of the Cimmerian Lhasa block with (Eur)Asia along the Bangong–Nujiang suture in Tibet (e.g. Yin and Harrison, 2000 and references therein). This suture continues to the Rushan–Pshart suture in the Pamirs (Ducea et al., 2003; Schwab et al., 2004). The collision–accretion of Lhasa again resulted in tectonic reactivation in the Tien Shan orogen (e.g. Hendrix et al., 1992; Allen et al., 1993; Graham et al., 1993; Otto, 1997; Dumitru et al., 2001; Vincent and Allen, 2001). We therefore interpret the Late Jurassic–Early Cretaceous cooling event from the northern Alai "basement" as denudation directly linked to the Lhasa collision (Fig. 9).

The younger, Late Cenozoic Trans-Alai sandstones (KYR-06 and KYR-07) do not contain a "typical Tien Shan" (Late Jurassic)–Early Cretaceous age population. However they do reveal a Late Cretaceous component (Figs. 6 and 9). This age component may be associated by yet another collision of Cimmerian or Tethyan terranes with southern (Eur)Asia that transpired chiefly in the "Pamir region" sensu lato. Several smaller blocks or a composite of these was accreted in the Tethyan Eurasian margin in the Late Cretaceous and principally involves the Karakoram block, the Koshistan Arc and the Hindu Kush. These basically form the backbone of the current Southern Pamirs (Ducea et al., 2003; Schwab et al., 2004) and amalgamation of these blocks induced tectonic activity in the current Pamir–Tien Shan transitional region, and invoked denudation and cooling of basement units and deposition of these "cooled" apatites in the Alai/Trans-Alai Basin where they define the detrital Late Cretaceous AFT component.

The latest Mesozoic and the Early Cenozoic for a large part represent a period of tectonic stability and quiescence with the

Author's personal copy

formation of a typical lateritic peneplanation surface across the Tien Shan (e.g. Burbank et al., 1999) and in the Ferghana Basin and adjoining ranges in particular (Bazhenov, 1993). No detrital age components from this period are found in our samples, nor do we find basement cooling ages in this time slice. The thermal history modeling of sample KYR-13 indeed describes a prolonged period of stability (Fig. 7) during which the apatites of this particular sample stayed more or less at the temperatures they had reached after cessation of the protracted Mesozoic reactivation and associated denudation – basement cooling events. For this specific sample, this implies that the apatites were kept at upper APAZ temperatures for the better part of ~100 Ma. This then caused the partial annealing of the fossil AFT lengths of the sample as observed in its length distribution (Fig. 7).

Finally, our data confirms that the current ongoing phase of cooling and denudation of the Alai basement commenced around 20–22 Ma ago, in the Early Miocene. Basement AFT cooling ages range from 22 to 8 Ma, basement AHe ages are situated between 12 and 5 Ma, thermal history modeling (AFT data KYR-13) shows basement cooling from ~20 Ma onwards, and lastly, detrital AFT ages show two Late Cenozoic age populations: (1) Early Miocene of ~18 Ma, and (2) Pliocene, ~3 Ma. This puts an absolute time frame on the Late Cenozoic evolution of the Alai segment of the Kyrgyz Southern Tien Shan (STS). The modern Turkestan, Alai and Kichi-Alai Ranges of the STS and the Tien Shan orogen as a whole, developed as a direct consequence of continued indentation of the Indian plate into the Eurasian continent. While convergence is accommodated through escape tectonics, mainly evident in Southeast Asia and Tibet, and by crustal thickening in the Himalayan orogen and the Tibetan Plateau, progressing strain is also partitioned to the intracontinental interior of Central Asia. In this way, the CAOB is being reactivated as a distal effect of India–Eurasia collision and has developed into the world's largest and most active intracontinental accretionary orogen. Miocene and Pliocene basement cooling and detrital age populations in other parts of the Tien Shan have been recognized by others as well (e.g. Hendrix et al., 1994; Sobel and Dumitru, 1997; Bullen et al., 2001; Dumitru et al., 2001; Sobel et al., 2006a,b; De Grave et al., 2008b; Wang et al., 2009a,b). The detrital age populations for the Trans-Alai samples presented in this paper (Figs. 6 and 9A) moreover correspond well with observations by Sonntag et al. (2010) and fits within the local tectonic frame work outlined by Coutand et al. (2002) and Strecker et al. (2003). In addition, Leloup et al. (2011) recently showed that strike-slip faulting along the Karakoram fault has been active since about 22–25 Ma ago. This fault zone is a major strike-slip zone along which the Pamir and Karakoram blocks are moving northward, converging toward the Tien Shan. As outlined in the introduction and geological setting section, a Late Cenozoic, in particular Miocene–Pliocene building of the modern Tien Shan is inferred from several lines of evidence and from various fields in geosciences. In particular successful in recent years magnetostratigraphic analysis of Neogene sedimentary sequences in the Tien Shan and adjoining basins have revealed pulsed denudation of the Tien Shan through the Miocene, Pliocene, and Pleistocene (e.g. Bullen et al., 2001; Charreau et al., 2006; Sun et al., 2007; Heermance et al., 2008 amongst others).

5. Conclusions

By using a multi-method geo- and thermochronology strategy in dating basement samples from the Alai-Turkestan region of the Kyrgyz Southern Tien Shan and detrital samples from the adjoining Ferghana Basin (north) and the Alai Basin/Trans-Alai Range (south), a consistent Late Palaeozoic to recent thermotectonic history can be reconstructed.

(1) Permian closure of the Turkestan Ocean between Tarim and the amalgamated palaeo-Kazakhstan with fringing Tien Shan units resulted in collision between these large blocks and formation of the ancestral Tien Shan orogen wedged in between. This collision is associated with large-scale emplacement of post-collision type granitoids across all boundaries of the composing Tien Shan units. In the Alai segment of the Kyrgyz Southern Tien Shan zircon U/Pb emplacement ages and thermal metamorphism ages of associated contact aureoles were found to be between ~284 and 263 Ma (Middle Permian).

(2) Carboniferous–Permian molasse units related to the aforementioned collision–accretion event were later buried under a thick blanket of Early–Middle Mesozoic sediments. Pre-existing apatite fission-track (AFT) information from the Permian units was consequently erased and the AFT "clock" was reset at that moment. Detrital apatites from Mesozoic sediments in the southeastern Ferghana Basin, yield Late Triassic source rock cooling ages of ~223 Ma. Younger, Late Cenozoic, sediments from the Trans-Alai Range also exhibit this Late Triassic age component, although it was found to be somewhat younger in that region (~207 Ma). Denudation of a reactivated Mesozoic Tien Shan orogen is thought to lie at the origin of this detrital AFT age component. The timing is coeval with the collision–accretion of the Cimmerian Qiangtang unit at the southern (Eur)Asian margin.

(3) Late Carboniferous–Permian molasse units at the present-day Ferghana Basin–Alai Range transition exhibit an Early Cretaceous apparent AFT age. When modeled using thermal history reconstruction software, these ages and the associated AFT length distributions predict an important Early Cretaceous cooling event (~140–110 Ma) affecting this area. This event exhumed the rocks near this basin–range transition to upper crustal levels. This exhumation event identifies a renewed pulse of Mesozoic Tien Shan reactivation and is contemporaneous with the collision–accretion of the Cimmerian Lhasa unit at the southern (Eur)Asian margin.

(4) Late Cenozoic sediments in the Trans-Alai Range contain a younger, Late Cretaceous detrital AFT age population of ~75 Ma. This implies that near the current Tien Shan–Pamir transition, source rocks were exhumed at that time and attained these Late Cretaceous cooling ages. This points to ongoing reactivation of the Tien Shan, simultaneous to accretion of the Karakoram block and associated units in the (Eur)Asian Tethyan margin.

(5) The modern Tien Shan orogen was constructed as a distal effect of India–Eurasia convergence in the Late Cenozoic. This important event is recorded both in the basement and the detrital apatite samples. Early Miocene AFT ages of the granitic basement are established at ~22 and 14 Ma and reveal the cooling of the basement as it is being exhumed and the eroded material is being deposited in the adjoining basins. A detrital age population of ~18 Ma can be found in the Trans-Alai. Moreover, when performing thermal history modeling on the Carboniferous–Permian molasse apatite sample with an apparent Early Cretaceous age, a relevant cooling episode initiating at around 20 Ma is revealed.

(6) Finally, one granite basement sample from the southern Alai Range yields a Late Miocene AFT age of ~8 Ma. A Pliocene age component of ~3 Ma is also present in the Trans Alai detrital samples. Late Miocene–Pliocene apatite (U–Th–Sm)/He cooling ages from the basement of the southern Alai Range imply final exhumation started between ~12 and 5 Ma.

Author's personal copy

Acknowledgements

The authors are supported by grants of the Fund for Scientific Research – Flanders (FWO, Belgium) (JDG) and the Institute for the Promotion of Innovation through Science and Technology in Flanders (IWT-Vlaanderen) (SG). This research was also co-funded by Ghent University (BOF – Bilateral Project 01SB1309). We are very grateful to Dr. Vladislav Yu. Batalev (International Research Center of the Russian Academy of Sciences in Bishkek, Kyrgyzstan), and other team-members for assistance during the field expeditions in 2005 and 2008. We are indebted to Dr. Guido Vittiglio and Dr. Peter Vermaercke for help with irradiations and neutron dosimetry at the Belgian Nuclear Research Centre in Mol (SCK-CEN, BR1 facility). We are very grateful to Dr. Daniel F. Stockli from Kansas State University for the apatite He analyses. Two anonymous reviewers are thanked for their insightful comments that helped to improve this paper. This paper is dedicated to our friend and colleague Alexander Ryabinin whose untimely passing in the Sayan Mountains will remain a life-long loss for us all.

References

Abdrakhmatov, K.Ye., Aldazhanov, S.A., Hager, B.H., Hamburger, M.W., Herring, T.A., Kalabaev, K.B., Makarov, V.I., Molnar, P., Panasyuk, S.V., Prilepin, M.T., Reilinger, R.E., Sadybakasov, I.S., Souter, B.J., Trapeznikov, Yu.A., Tsurkov, V.Ye., Zubovich, A.V., 1996. Relatively recent construction of the Tien Shan inferred from GPS measurements of present-day crustal deformation. Nature 384, 450–453.

Alekseev, D.V., Aristov, V.A., Degtyarev, K.E., 2007. The age and tectonic setting of volcanic and cherty sequences in the ophiolite complex of the Atbashe Ridge (Southern Tien Shan). Doklady Earth Sciences 413A, 380–383.

Alekseev, D.V., Degtyarev, K.E., Kotov, A.B., Sal'nikova, E.B., Tret'yakov, A.A., Yakovleva, S.Z., Anisimova, I.V., Shatagin, K.N., 2009. Late Paleozoic subductional and collisional igneous complexes in the Naryn Segment of the Middle Tien Shan (Kyrgyzstan). Doklady Earth Sciences 427, 760–763.

Allen, M.B., Vincent, S.J., 1997. Fault reactivation in the Junggar region, northwest China: the role of basement structures during Mesozoic–Cenozoic compression. Journal of the Geological Society, London 154, 151–155.

Allen, M.B., Windley, B.F., Chi, Zhang., 1992. Palaeozoic collisional tectonics and magmatism of the Chinese Tien Shan, Central Asia. Tectonophysics 220, 89–115.

Allen, M.B., Windley, B.F., Chi, Zhang., Guo, J., 1993. Evolution of the Turfan Basin, Chinese Central Asia. Tectonics 12, 889–896.

Allen, M.B., Şengör, A.M.C., Natal'in, B.A., 1995. Junggar, Turfan and Alakol basins as Late Permian to ? Early Triassic extensional structures in a sinistral shear zone in the Altaid orogenic collage, Central Asia. Journal of the Geological Society, London 152, 327–338.

Allen, M.B., Vincent, S.J., Wheeler, P.J., 1999. Late Cenozoic tectonics of the Kepingtage thrust zone: interactions of the Tien Shan and Tarim Basin, northwest China. Tectonics 18, 639–654.

Allen, M.B., Alsop, G.I., Zhemchuzhnikov, V.G., 2001. Dome and basin refolding and transpressive inversion along the Karatau fault System, southern Kazakstan. Journal of the Geological Society, London 158, 83–95.

Bazhenov, M.L., 1993. Cretaceous paleomagnetism of the Fergana Basin and adjacent ranges, Central Asia: tectonic implications. Tectonophysics 221, 251–267.

Biske, Yu.S., Seltmann, R., 2010. Paleozoic Tian-Shan as a transitional region between the Rheic and Urals-Turkestan oceans. Gondwana Research 17, 602–613.

Bullen, M.E., Burbank, D.W., Garver, J.I., Abdrakhmatov, K.Ye., 2001. Late Cenozoic tectonic evolution of the northwestern Tien Shan: new age estimates for the initiation of mountain building. Geological Society of America Bulletin 113, 1544–1559.

Burbank, D.W., McLean, J.K., Bullen, M., Abdrakhmatov, K.Y., Miller, M.M., 1999. Partitioning of intramontane basins by thrust related folding, Tien Shan, Kyrgyzstan. Basin Research 11, 75–92.

Burov, E.B., Kogan, M.G., Lyon-Caen, H., Molnar, P., 1990. Gravity anomalies, the deep structure, and dynamic processes beneath the Tien Shan. Earth and Planetary Science Letters 96, 367–383.

Burtman, V.S., Skobelev, S.F., Molnar, P., 1996. Late Cenozoic slip on the Talas-Ferghana fault, the Tien Shan, central Asia. Geological Society of America Bulletin 108, 1004–1021.

Buslov, M.M., Klerkx, J., Abdrakhmatov, K., Delvaux, D., Batalev, V. Yu., Kuchai, O.A., Dehandschutter, B., Muraliev, A., 2003a. Recent strike-slip deformation of the northern Tien Shan. In: Storti, F., Holdsworth, R.E., Salvini, F. (Eds.), Intraplate Strike-Slip Deformation Belts. Geological Society of London, Special Publication 210, pp. 53–64.

Buslov, M.M., Watanabe, T., Smirnova, L.V., Fujiwara, I., Iwata, K., De Grave, J., Semakov, N.N., Travin, A.V., Kiryanova, A.P., Kokh, D.A., 2003b. Role of strike-slip faults in Late Paleozoic–Early Mesozoic tectonics and geodynamics of the Altai-Sayan and East Kazakhstan folded zone. Russian Geology and Geophysics 44, 49–75.

Carlson, W.D., Donelick, R.A., Ketcham, R.A., 1999. Variability of apatite fission-track annealing kinetics: I. Experimental results. American Mineralogist 84, 1213–1223.

Carroll, A.R., Graham, S.A., Hendrix, M.S., Ying, D., Zhou, D., 1995. Late Paleozoic tectonic amalgamation of northwestern China: sedimentary record of the northern Tarim, northwestern Turpan and southern Junggar basins. Geological Society of America Bulletin 107, 571–594.

Charreau, J., Gilder, S., Chen, Y., Dominguez, S., Avouac, J.-P., Sen, S., Jolivet, M., Li, Y., Wang, W., 2006. Magnetostratigraphy of the Yaha section, Tarim basin, China): 11 Ma acceleration in erosion and uplift of the Tian Shan mountains. Geology 34, 181–184.

Chiaradia, M., Konopelko, D., Seltmann, R., Cliff, R.A., 2006. Lead isotope variations across terrane boundaries of the Tien Shan and Chinese Altay. Mineralium Deposita 41, 411–428.

Cobbold, P.R., Sadybakasov, E., Thomas, J.C., 1994. Cenozoic transpression and basin development, Kyrghyz Tienshan, Central Asia. In: Roure, F., Ellouz, N., Shein, V.S., Skvortsov, I. (Eds.), Geodynamic Evolution of Sedimentary Basins, International Symposium, Moscow, pp. 181–202.

Coutand, I., Strecker, M.R., Arrowsmith, J.R., Hilley, G., Thiede, R.C., Korjenkov, A., Omuraliev, M., 2002. Late Cenozoic tectonic development of the intramontane Alai Valley (Pamir–Tien Shan region, central Asia): an example of intracontinental deformation due to the Indo-Eurasia collision. Tectonics 21, 1053, 19 pp.

De Corte, F., Bellemans, F., Van den haute, P., Ingelbrecht, C., Nicholl, C., 1998. A new U doped glass certified by the European Commission for the calibration of fission-track dating. In: Van den haute, P., De Corte, F. (Eds.), Advances in Fission-Track Geochronology. Kluwer Academic Publishers, Dordrecht, pp. 67–78.

De Grave, J., Van den haute, P., 2002. Denudation and cooling of the Lake Teletskoye region in the Altai Mountains (South Siberia) as revealed by apatite fission-track thermochronology. Tectonophysics 349, 145–159.

De Grave, J., Buslov, M.M., Van den haute, P., 2007. Distant effects of India–Eurasia convergence and Mesozoic intracontinental deformation in Central Asia: constraints from apatite fission-track thermochronology. Journal of Asian Earth Sciences 29, 188–204.

De Grave, J., Van den haute, P., Buslov, M.M., Dehandschutter, B., Glorie, S., 2008a. Apatite fission-track thermochronology applied to the Chulyshman Plateau, Siberian Altai Region. Radiation Measurements 43, 38–42.

De Grave, J., Buslov, M.M, Glorie, S., Stockli, D.F., Van den haute, P., Batalev, V.Y., Kislitsyn, R.V., McWilliams, M.O., 2008b. Thermochronology of the Kyrgyz Tien Shan reveals the timing of punctuated Late Triassic to Late Cretaceous Tethyian subduction and Tibetan collisions and of Cenozoic mountain building as response to India–Eurasia convergence. In: Garver, J.I., Montario, M.J. (Eds.), Proceedings from the 11th International Conference on Thermochronometry, Anchorage, AK, USA, 15-19/09/2008, pp. 54–57.

De Grave, J., Buslov, M.M., Van den haute, P., Metcalf, J., Dehandschutter, B., Mc Williams, M.O., 2009. Multi-method chronometry of the Teletskoye graben and its basement, Siberian Altai Mountains: new insights on its thermo-tectonic evolution. In: Lisker, F., Ventura, B., Glasmacher, U.A. (Eds.), Thermochronological Methods from Palaeotemperature Constraints to Landscape Evolution Models. The Geological Society of London Special Publication 324, pp. 237–259.

De Grave, J., Glorie, S., Vermaercke, P., Vittiglio, G., Van den haute, P., 2010. A "new" irradiation facility for FT applications at the Belgian Nuclear Research Centre: the BR1 Reactor. In: Abstract, Thermo2010, 12th International Conference on Thermochronology, p. 119.

Ducea, M.N., Lutkov, V., Minaev, V.T., Hacker, B., Ratschbacher, L., Luffi, P., Schwab, M., Gehrels, G.E., McWilliams, M., Vervoort, J., Metcalf, J., 2003. Building the Pamirs: the view from the underside. Geology 31, 849–852.

Dumitru, T.A., Zhou, D., Chang, E.Z., Graham, S.A., 2001. Uplift, exhumation, and deformation in the Chinese Tian Shan. Geological Society of America Memoir 194, 71–99.

Dunkl, I., Mikes, T., Frei, D., Gerdes, A., von Eynatten, H., 2009. PepiAGE: Data Reduction Program for Time-Resolved U/Pb Analyses – Introduction and Call for Tests and Discussion. University of Goettingen Publication, 15 pp. <http://www.sediment.uni-goettingen.de/staff/dunkl/zips/PepiAGE-introduction-c1.pdf>.

Ehlers, T.A., Farley, K.A., 2003. Apatite (U–Th)/He thermochronometry: methods and applications to problems in tectonic and surface processes. Earth and Planetary Science Letters 206, 1–14.

Farley, K.A., 2002. (U–Th)/He dating: techniques, calibrations, and applications. Noble Gas Geochemistry, Reviews in Mineralogy and Geochemistry 47, 819–844.

Farley, K.A., Stockli, D.F., 2002. (U–Th)/He dating of phosphates: apatite, monazite, and xenotime. Phosphates: Geochemical, Geobiological, and Materials Importance, Reviews in Mineralogy and Geochemistry 48, 559–577.

Farley, K.A., Wolf, R.A., Silver, L.T., 1996. The effects of long alpha-stopping distances on (U–Th)/He ages. Geochimica et Cosmochimica Acta 60, 4223–4229.

Frei, D., Gerdes, A., 2009. Accurate and precise in-situ zircon U–Pb age dating with high spatial resolution and high sample throughput by automated LA-SF-ICP-MS. Chemical Geology 261, 261–270.

Galliker, D., Hugentobler, E., Hahn, B., 1970. Spontane kernspaltung von ^{238}U und ^{241}Am. Helveticae Physicae Acta 43, 593–606.

Gao, J., Maosong, Li., Xuchang, Xiao., Yaoqing, Tang., Guoqi, He., 1998. Paleozoic tectonic evolution of the Tienshan orogen, northwestern China. Tectonophysics 287, 213–231.

Author's personal copy

Gao, J., Long, L.L., Klemd, R., Qian, Q., Liu, D.Y., Xiong, X.M., Su, W., Liu, W., Wang, Y.T., Yang, F.Q., 2009. Tectonic evolution of the South Tianshan orogen and adjacent regions, NW China: geochemical and age constraints of granitoid rocks. International Journal of Earth Science 98, 1221–1238.

Gleadow, A.J.W., Duddy, I.R., Green, P.F., Lovering, J.F., 1986. Confined fission track lengths in apatite: a diagnostic tool for thermal history analysis. Contributions to Mineralogy and Petrology 94, 405–415.

Glorie, S., De Grave, J., Buslov, M.M., Elburg, M.A., Stockli, D.F., Van den haute, P., Gerdes, A., 2010a. Multi-method chronometric constraints on the evolution of the Northern Kyrgyz Tien Shan batholith: from emplacement to exhumation. Journal of Asian Earth Sciences 38, 131–146.

Glorie, S., De Grave, J., Van den haute, P., Elburg, M.A., 2010b. Evaluating the effect of anisotropy on fossil fission track length distributions in apatite. In: Abstract, Thermo2010, 12th International Conference on Thermochronology, p. 120.

Glorie, S., De Grave, J., Buslov, M.M., Zhimulev, F.I., Izmer, A., Vandoorne, W., Ryabinin, A., Van den haute, P., Elburg, M.A., in press. Formation and Palaeozoic evolution of the Gorny-Altai–Altai-Mongolia suture zone (South Siberia): zircon U/Pb constraints on the igneous record. Gondwana Research. doi:10.1016/j.gr.2011.03.003.

Graham, S.A., Hendrix, M.S., Wang, L.B., Carroll, A.R., 1993. Collisional successor basins of western China: impact of tectonic inheritance on sand composition. Geological Society of America Bulletin 105, 323–344.

Green, P.F., Duddy, I.R., Gleadow, A.J.W., Tingate, P.R., Laslett, G.M., 1986. Thermal annealing of fission tracks in apatite.1. A qualitative description.. Chemical Geology (Isotopes Geoscience Section) 59, 237–253.

Hasebe, N., Barabarand, J., Jarvis, K., Carter, A., Hurford, A.J., 2004. Apatite fission-track chronometry using laser ablation ICP-MS. Chemical Geology 207, 135–145.

Heermance, R.V., Chen, J., Burbank, D.B., Miao, J., 2008. Temporal constraints and evidence for pulsed Late Cenozoic deformation during the structural disruption of the active Kashi foreland, northwest China. Tectonics 27, TC6012. doi:10.1029/2007TC002226.

Hendrix, M.S., 2000. Evolution of Mesozoic sandstone compositions, southern Junggar, northern Tarim, and western Turpan basins, northwest China: a detrital record of the ancestral Tian Shan. Journal of Sedimentary Research 70, 520–532.

Hendrix, M.S., Graham, S.A., Carroll, A.R., Sobel, E.R., McKnight, C.L., Schulein, B.J., Wang, Z., 1992. Sedimentary record and climatic implications of recurrent deformation in the Tian Shan: evidence from Mesozoic strata of the north Tarim, south Junggar, and Turpan basins, NW China. Geological Society of America Bulletin 104, 53–79.

Hendrix, M.S., Dumitru, T.A., Graham, S.A., 1994. Late Oligocene–Early Miocene unroofing in the Chinese Tien Shan: an early effect of the India–Asia collision. Geology 22, 487–490.

Heubeck, C., 2001. Assembly of central Asia during the middle and late Paleozoic. Geological Society of America Memoir 194, 1–22.

Horstwood, M.S.A., Foster, G.L., Parrish, R.R., Noble, S.R., Nowell, G.R., 2003. Common-Pb corrected in situ U–Pb accessory mineral geochronology by LA-MC-ICPMS. Journal of Analytical Atomic Spectroscopy 18, 837–846.

House, M.A., Farley, K.A., Stockli, D., 2000. Helium chronometry of apatite and titanite using Nd-YAG laser heating. Earth and Planetary Science Letters 183, 365–368.

Hubert-Ferrari, A., Suppe, J., Gonzalez-Mieres, R., Wang, X., 2007. Mechanisms of active folding of the landscape (southern Tian Shan, China). Journal of Geophysical Research 112, B03S09.

Hurford, A.J., 1990. Standardization of fission track dating calibration: recommendation by the Fission Track Working Group of the IUGS Subcommission on Geochronology. Chemical Geology (Isotope Geoscience Section) 80, 171–178.

Izmer, A., Glorie, S., De Grave, J., Vanhaecke, F., Elburg, M., 2010. Precise in situ zircon U/Pb dating by LA-SF-ICP-MS: comparison of two different laser systems. In: Abstract book of the 10th European Workshop on Laser Ablation, Kiel, Germany, p. 90.

Jackson, S.E., Pearson, N.J., Griffin, W.L., Belousova, E.A., 2004. The application of laser ablation-inductively coupled plasma-mass spectrometry to in situ U–Pb zircon geochronology. Chemical Geology 211, 47–69.

Jaffey, A.H., Flynn, K.F., Glendenin, L.E., Bentley, W.C., Essling, A.M., 1971. Precission measurements of half-lives and specific activities of ^{325}U and ^{238}U. Physical Review C4, 1889–1906.

Jenchuraeva, R., Bakirov, A., Ghes, M., Seltmann, R., Shatov, V., Popov, V., 2001. Mineral Deposits Map of Kyrgyzstan, 1:1000,000. International Association on the Genesis of Ore Deposits, London-Bishkek.

Jochum, K.P., Stoll, B., 2008. Reference materials for elemental and isotopic analyses by LA-(MC)-ICPMS: successes and outstanding needs. In: Sylvester, P. (Ed.), Short Course Series, vol. 40. Mineralogical Association of Canada, Ottawa, Canada, pp. 147–168.

Jolivet, M., Dominguez, S., Charreau, J., Chen, Y., Li, Y., Wang, Q., 2010. Mesozoic and Cenozoic tectonic history of the central Chinese Tian Shan: reactivated tectonic structures and active deformation. Tectonics 29. doi:10.1029/2010TC002712.

Jonckheere, R., Enkelmann, E., Min, M., Trautmann, C., Ratschbacher, L., 2007. Confined fission tracks in ion-irradiated and step-etched prismatic sections of Durango apatite. Chemical Geology 242, 202–217.

Kapp, P., DeCelles, P.G., Gehrels, G.E., Heizler, M., Ding, L., 2007. Geological records of the Lhasa-Qiangtang and Indo-Asian collisions in the Nima area of central Tibet. Geological Society of America Bulletin 119, 917–932.

Ketcham, R.A., 2005. Forward and inverse modeling of low-temperature thermochronometry data. Reviews in Mineralogy and Geochemistry 58, 275–314.

Ketcham, R.A., Carter, A., Donelick, R.A., Barbarand, J., Hurford, A.J., 2007. Improved modelling of fission-track annealing in apatite. American Mineralogist 92, 799–810.

Konopelko, D., Biske, G., Seltmann, R., Eklund, O., Belyatsky, B., 2007. Hercynian post-collisional A-type granites of the Kokshaal Range, Southern Tien Shan, Kyrgyzstan. Lithos 97, 140–160.

Konopelko, D., Biske, G., Seltmann, R., Kiseleva, M., Matukov, D., Sergeev, S., 2008. Deciphering Caledonian events: timing and geochemistry of the Caledonian magmatic arc in the Kyrgyz Tien Shan. Journal of Asian Earth Sciences 32, 131–141.

Konopelko, D., Seltmann, R., Biske, G., Lepekhina, E., Sergeev, S., 2009. Possible source dichotomy of contemporaneous post-collisional barren I-type versus tin-bearing A-type granites, lying on opposite sides of the South Tien Shan suture. Ore Geology Reviews 35, 206–216.

Laurent-Charvet, S., Charvet, J., Shu, L., Ma, R., Lu, H., 2002. Palaeozoic late collisional strike-slip deformations in Tianshan and Altay, Eastern Xinjiang, NW China. Terra Nova 14, 249–256.

Leloup, P.H., Boutonnet, E., Davis, W.J., Hattori, K., 2011. Long-lasting intracontinental strike-slip faulting: new evidence from the Karakorum shear zone in the Himalayas. Terra Nova 23, 92–99.

Long, L., Gao, J., Wang, J., Qian, Q., Xiong, X., Wang, Y., Wang, L., Gao, L., 2008. Geochemistry and SHRIMP zircon U–Pb age of post-collisional granites in the Southwest Tianshan orogenic belt of China: example from the Heiyingshan and Laohutai plutons. Acta Geologica Sinica 82, 415–424.

Ludwig, K., 2003. User's Manual for Isoplot 3.00, A Geochronological Toolkit for Microsoft Excel, vol. 4. Berkeley Geochronology Center Special Publication.

Mao, J., Konopelko, D., Seltmann, R., Lehmann, B., Chen, W., Wang, Y., Eklund, O., Usubaliev, T., 2004. Postcollisional age of the Kumtor gold deposit and timing of Hercynian events in the Tien Shan, Kyrgyzstan. Economic Geology 99, 1771–1780.

McDowell, F.W., McIntosh, W.C., Farley, K.A., 2005. A precise ^{40}Ar/^{39}Ar reference age for the Durango apatite (U-Th)/He and fission-track dating standard. Chemical Geology 214, 249–263.

Min, M., Enkelmann, E., Jonckheere, R., Trautmann, C., Ratschbacher, L., 2007. Measurements of fossil confined fission tracks in ion-irradiated apatite samples with low track densities. Nuclear Instruments and Methods in Physics Research B 259, 943–950.

Molnar, P., Tapponnier, P., 1975. Cenozoic tectonics of Asia: effects of a continental collision. Science 189, 419–426.

Morelli, R., Creaser, R.A., Seltmann, R., Stuart, F.M., Selby, D., Graupner, T., 2007. Age and source constraints for the giant Muruntau gold deposit, Uzbekistan, from coupled Re–Os–He isotopes in arsenopyrite. Geology 35, 795–798.

Omuralieva, A., Nakajima, J., Hasegawa, A., 2009. Three-dimensional seismic velocity structure of the crust beneath the central Tien Shan, Kyrgyzstan: Implications for large- and small-scale mountain building. Tectonophysics 465, 30–44.

Oskin, M.E., Burbank, D., 2007. Transient landscape evolution of basement-cored uplifts: example of the Kyrgyz Range, Tian Shan. Journal of Geophysical Research 112, F03S03, 20 pp.

Otto, S.C., 1997. Mesozoic–Cenozoic history of deformation and petroleum systems in sedimentary basins of Central Asia: implications of collisions on the Eurasian margin. Petroleum Geoscience 3, 327–341.

Pavlis, T.L., Hamburger, M.W., Pavlis, G.L., 1997. Erosional processes as a control on the structural evolution of an actively deforming fold and thrust belt: an example from the Pamir–Tien Shan region, central Asia. Tectonics 16, 810–822.

Pickering, K.T., Koren, T.N., Lytochkin, V.N., Siveter, D.J., 2008. Silurian–Devonian active-margin deep-marine systems and paleogeography, Alai Range, Southern Tien Shan, Central Asia. Journal of the Geological Society of London 165, 189–210.

Robinson, A.C., Yin, A., Manning, C.E., Harrison, T.M., Zhang, S.-H., Wang, X.-F., 2007. Cenozoic evolution of the eastern Pamir: implications for strain-accommodation mechanisms at the western end of the Himalayan–Tibetan orogen. Geological Society of America Bulletin 119, 882–896.

Schwab, M., Ratschbacher, L., Siebel, W., McWilliams, M., Minaev, V., Lutkov, V., Chen, F., Stanek, K., Nelson, B., Frisch, F., Wooden, J.L., 2004. Assembly of the Pamirs: age and origin of magmatic belts from the southern Tien Shan to the southern Pamirs and their relation to Tibet. Tectonics 23, TC4002. doi:10.1029/2003TC001583, 31 pp.

Seifert, W., Kämpf, H., Wasternack, J., 2000. Compositional variation in apatite, phlogopite and other accessory minerals of the ultramafic Delitzsch complex, Germany: implication for cooling history of carbonatites. Lithos 53, 81–100.

Seltmann, R., Konopelko, D., Biske, G., Divaev, F., Sergeev, S., 2011. Hercynian post-collisional magmatism in the context of Paleozoic magmatic evolution of the Tien Shan orogenic belt. Journal of Asian Earth Sciences 42, 821–838.

Simonov, V.A., Sakiev, K.S., Volkova, N.I., Stupakov, S.I., Travin, A.V., 2008. Conditions of formation of the Atbashi Ridge eclogites (South Tien Shan). Russian Geology and Geophysics 49, 803–815.

Sláma, J., Košler, J., Condon, D.J., Crowley, J.L., Gerdes, A., Hanchar, J.M., Horstwood, M.S.A., Morris, G.A., Nasdala, L., Norberg, N., Schaltegger, U., Schoene, B., Tubrett, M.N., Whitehouse, M.J., 2008. Plešovice zircon – a new natural reference material for U–Pb and Hf isotopic microanalysis. Chemical Geology 249, 1–35.

Author's personal copy

Sobel, E.R., Dumitru, T.A., 1997. Thrusting and exhumation around the margins of the western Tarim Basin during the India–Asia collision. Journal of Geophysical Research 102, 5043–5064.
Sobel, E., Chen, J., Heermance, R.V., 2006a. Late Oligocene–Early Miocene initiation of shortening in the SW Chinese Tian Shan: implications for Neogene shortening rate variations. Earth and Planetary Science Letters 247, 70–81.
Sobel, E.R., Oskin, M., Burbank, D., Mikolaichuk, A., 2006b. Exhumation of basement-cored uplifts: example of the Kyrgyz Range quantified with apatite fission track thermochronology. Tectonics 25, 1–17.
Solomovich, L.I., 2007. Postcollisional magmatism in the South Tien Shan Variscan Orogenic Belt, Kyrgyzstan: evidence for high-temperature and high-pressure collision. Journal of Asian Earth Sciences 30, 142–153.
Solomovich, L.I., Trifonov, B.A., 2002. Postcollisional granites in the South Tien Shan Variscan Collisional Belt, Kyrgyzstan. Journal of Asian Earth Sciences 21, 7–21.
Sonntag, B.-L., Hofmann, J., Schmalholz, M., Lohr, T., Ratschbacher, L., Jonckheere, R., 2010. Geometry and age of intra-continental shortening along the Alai valley, Pamir–Tien Shan, Central Asia. In: Abstract, Thermo2010, 12th International Conference on Thermochronology, p. 280.
Stacey, J.S., Kramers, J.D., 1975. Approximation of terrestrial lead isotope evolution by a two-stage model. Earth and Planetary Science Letters 26, 207–221.
Steiger, R.H., Jäger, E., 1977. Subcommission on Geochronology: convention on the use of decay constants in geo- and cosmochronology. Earth and Planetary Science Letters 36, 359–362.
Stockli, D.F., Farley, K.A., Dumitru, T.A., 2000. Calibration of the apatite (U–Th)/He thermochronometer on an exhumed fault block, White Mountains, California. Geology 28, 983–986.
Strecker, M.R., Hilley, G.E., Arrowsmith, J.R., Coutand, I., 2003. Differential structural and geomorphic mountain-front evolution in an active continental collision zone: the northwest Pamir, southern Kyrgyzstan. Geological Society of America Bulletin 115, 166–181.
Sun, J., Xu, Q., Huang, B., 2007. Late Cenozoic magnetochronology and paleoenvironmental changes in the northern foreland basin of the Tian Shan Mountains. Journal of Geophysical Research 112, B04107, 14 pp.
Tursungaziev, B.T., Petrov, O.B. (Eds.), 2008. Geological Map of the Kyrgyz Republic, 1:500,000. Bishkek.
Van den haute, P., De Corte, F., Jonckheere, R., Bellemans, F., 1998. The parameters that govern the accuracy of fission-track age determinations: a re-appraisal. In: Van den haute, P., De Corte, F. (Eds.), Advances in Fission-Track Geochronology. Kluwer Academic Publishers, Dordrecht, pp. 33–46.
Van der Voo, R., Levashova, N.M., Skrinnik, L.I., Kara, T.V., Bazhenov, M.L., 2006. Late orogenic, large-scale rotations in the Tien Shan and adjacent mobile belts in Kyrgyzstan and Kazakhstan. Tectonophysics 426, 335–360.
Vermeesch, P., 2009. RadialPlotter: a Java application for fission track, luminescence and other radial plots. Radiation Measurements 44, 409–410.
Vincent, S.J., Allen, M.B., 2001. Sedimentary record of Mesozoic intracontinental deformation in the eastern Junggar Basin, northwest China: response to orogeny at the Asian margin. Geological Society of America Memoir 194, 341–360.
Wagner, G.A., Van den haute, P., 1992. Fission Track-Dating. Kluwer Academic Publishers, Dordrecht, 285 pp.
Wang, B., Cluzel, D., Shu, L.S., Faure, M., Charvet, J., Chen, Y., Meffre, S., de Jong, K., 2009a. Evolution of calc-alkaline to alkaline magmatism through Carboniferous convergence to Permian transcurrent tectonics, western Chinese Tianshan. International Journal of Earth Science 98, 1275–1298.
Wang, Q., Li, S., Du, Z., 2009b. Differential uplift of the Chinese Tianshan since the Cretaceous: constraints from sedimentary petrography and apatite fission-track dating. International Journal of Earth Science 98, 1341–1363.
Wiedenbeck, M., Alle, P., Corfu, F., Griffin, W., Meier, M., Oberli, F., von Quadt, A., Roddick, J.C., Spiegel, W., 1995. Three natural zircon standards for U–Th–Pb, Lu–Hf, trace element and REE analysis. Geostandards Newsletter 19, 1–23.
Windley, B.F., Alexeiev, D., Xiao, W., Kröner, A., Badarch, G., 2007. Tectonic models for accretion of the Central Asian Orogenic Belt. Journal of the Geological Society of London 164, 31–47.
Xiao, W.J., Huang, B.C., Han, C.M., Sun, S., Li, J.L., 2010. A review of the western part of the Altaids: a key to understanding the architecture of accretionary orogens. Gondwana Research 18, 253–273.
Yang, Y., Liu, M., 2002. Cenozoic deformation of the Tarim plate and the implications for mountain building in the Tibetan Plateau and the Tian Shan. Tectonics 21, 1059. doi:10.1029/2001TC001300, 17 pp.
Yin, A., Harrison, T.M., 2000. Geological evolution of the Himalayan–Tibetan orogen. Annual Review in Earth and Planetary Sciences 28, 211–280.
Yin, A., Nie, S., Craig, P., Harrison, T.M., Ryerson, F., Qian, X., Yang, G., 1998. Late Cenozoic tectonic evolution of the southern Chinese Tian Shan. Tectonics 17, 1–27.
Ziegler, J.F., Biersack, J.P., Littmark, U., 1985. The Stopping and Range of Ions in Solids. Pergamon Press, New York, 321 pp.